Photoproduction of $\pi^+\pi^-$ pairs in a model with tensor-pomeron and vector-odderon exchange

Arthur Bolz,[a] **Carlo Ewerz,**[b,c] **Markos Maniatis,**[d] **Otto Nachtmann,**[b] **Michel Sauter**[a] **and André Schöning**[a]

[a]*Physikalisches Institut, Universität Heidelberg,*
Im Neuenheimer Feld 226, D-69120 Heidelberg, Germany

[b]*Institut für Theoretische Physik, Universität Heidelberg,*
Philosophenweg 16, D-69120 Heidelberg, Germany

[c]*ExtreMe Matter Institute EMMI, GSI Helmholtzzentrum für Schwerionenforschung,*
Planckstraße 1, D-64291 Darmstadt, Germany

[d]*Departamento de Ciencias Básicas, Universidad del Bío-Bío,*
Avda. Andrés Bello s/n, Casilla 447, Chillán 3780000, Chile

E-mail: abolz@physi.uni-heidelberg.de,
C.Ewerz@thphys.uni-heidelberg.de, mmaniatis@ubiobio.cl,
O.Nachtmann@thphys.uni-heidelberg.de, Michel.Sauter@desy.de,
schoening@physi.uni-heidelberg.de

ABSTRACT: We consider the reaction $\gamma p \to \pi^+\pi^- p$ at high energies. Our description includes dipion production via the resonances ρ, ω, ρ' and f_2, and via non-resonant mechanisms. The calculation is based on a model of high energy scattering with the exchanges of photon, pomeron, odderon and reggeons. The pomeron and the $C = +1$ reggeons are described as effective tensor exchanges, the odderon and the $C = -1$ reggeons as effective vector exchanges. We obtain a gauge-invariant version of the Drell-Söding mechanism which produces the skewing of the ρ-meson shape. Starting from the explicit formulae for the matrix element for dipion production we construct an event generator which comprises all contributions mentioned above and includes all interference terms. We give examples of total and differential cross sections and discuss asymmetries which are due to interference of $C = +1$ and $C = -1$ exchange contributions. These asymmetries can be used to search for odderon effects. Our model is intended to provide all necessary theoretical tools for a detailed experimental analysis of elastic dipion production for which data exist from fixed target experiments, from HERA, and are now being collected by LHC experiments.

KEYWORDS: QCD Phenomenology, Phenomenological Models

Contents

1 Introduction

Photoproduction of $\pi^+\pi^-$ pairs on protons at high energies, that is the reaction

$$\gamma(q) + p(p) \longrightarrow \pi^+(k_1) + \pi^-(k_2) + p(p') \,, \tag{1.1}$$

has been studied for a long time, both in theory and experiment. For reviews of topics relevant for this reaction see, for instance, [1–3], and for model calculations [4–6], for example. The reaction (1.1) has been investigated by fixed target experiments [7–15] and by the experiments H1 and ZEUS at HERA [16–18]. A related reaction is the central exclusive production of a $\pi^+\pi^-$ pair in ultra-peripheral pp, Ap, and AA collisions; cf. [19–22]. Results for AA collisions are available from the STAR collaboration at RHIC [23–26] and from the ALICE collaboration at LHC [27]. In the present paper we shall, however, only deal with the γp reaction (1.1). The purpose of our paper is to give detailed formulae for the reaction (1.1) as obtained in the recently proposed model [28]. This model is constructed

to describe soft high-energy reactions including Regge behaviour of the amplitudes. The pomeron and the charge conjugation $C = +1$ reggeons are described as effective tensor-exchange objects, the odderon and the $C = -1$ reggeons as effective vector-exchange objects. Due to these properties the amplitudes obtained in the model [28] naturally satisfy the rules of quantum field theory. In particular, they exhibit the correct behaviour under crossing and under charge conjugation.

The reaction (1.1) offers the interesting possibility to find odderon effects. Let us, therefore, first discuss the status of the odderon. The odderon, the charge conjugation $C = -1$ counterpart of the $C = +1$ pomeron, was introduced on theoretical grounds in [29, 30]. More than forty years after its introduction the odderon is seen in theoretical papers, but not yet clearly in experiments. For a review see [31]; for a general discussion of the pomeron and the odderon in high-energy reactions and QCD see [2]. Various reactions have been proposed in order to look for odderon effects. We are concerned here with two of these proposals. One, suggested in [32–36], is to study the exclusive photoproduction of $C = +1$ mesons and in particular the production of the $f_2 \equiv f_2(1270)$ meson. The other is to look for certain asymmetries of the final state caused by the interference of C-even and C-odd exchanges. Various asymmetries of this kind have been described in [37–44]. For a review of these and other observables suited for odderon searches see [31].

We shall discuss now the relevant production mechanisms and diagrams for the reaction (1.1) for high energies, $s \gg m_p^2$, and for $\pi^+\pi^-$ invariant mass, $m_{\pi^+\pi^-}$, from threshold to $m_{\pi^+\pi^-} \approx 2\,\text{GeV}$. The kinematic quantities for this reaction are collected in appendix A. In this kinematic region we expect to see the production of the ρ meson, including ρ–ω interference effects, and the resonant production of the f_2 and $\rho' \equiv \rho(1450)$ mesons. The exchanges to be considered are: the pomeron $\mathbb{P}$, the reggeons f_{2R}, a_{2R}, ω_R, ρ_R, the photon γ and — if it exists — the odderon $\mathbb{O}$. In addition to resonance production, the $\pi^+\pi^-$ continuum production is considered. The diagrams for all these subprocesses are shown in figure 1. In the following these diagrams are evaluated in the model presented in [28] and we shall give explicit formulae which can serve as basis for experimental analyses. The photoproduction of a neutral meson by photon exchange is called the Primakoff effect [45]. Our diagram 1(c) corresponds to this effect with f_2 as the neutral meson. We see from figure 1 that exchanges with $C = +1$ ($\mathbb{P}$, f_{2R}, a_{2R}) and $C = -1$ (ω_R, ρ_R, γ, $\mathbb{O}$) contribute to the reaction (1.1). This leads to asymmetries in the $\pi^+\pi^-$ distributions, as we shall discuss at length below. Such asymmetries have been proposed for odderon searches in [38–44]. But, as we see from figure 1, odderon exchange is not the only $C = -1$ exchange contribution. Thus, a careful analysis of all contributing $C = +1$ and $C = -1$ exchanges is necessary in order to assess the rôle of the odderon. In this paper we present such a description as is a prerequisite for an experimental search for odderon effects in the reaction (1.1).

Before we do this we give an argument why the photoproduction of f_2 mesons may be particularly sensitive to odderon effects. We show in figure 2 a QCD diagram which contributes and is specific to f_2 production. Via loops the photon γ can couple to three gluons and the f_2 can couple to two gluons, resulting with proper arrangement of the gluon lines in a three-gluon exchange (the simplest perturbative representation of the odderon) with the proton. We note that this type of diagram does not exist for the photoproduction
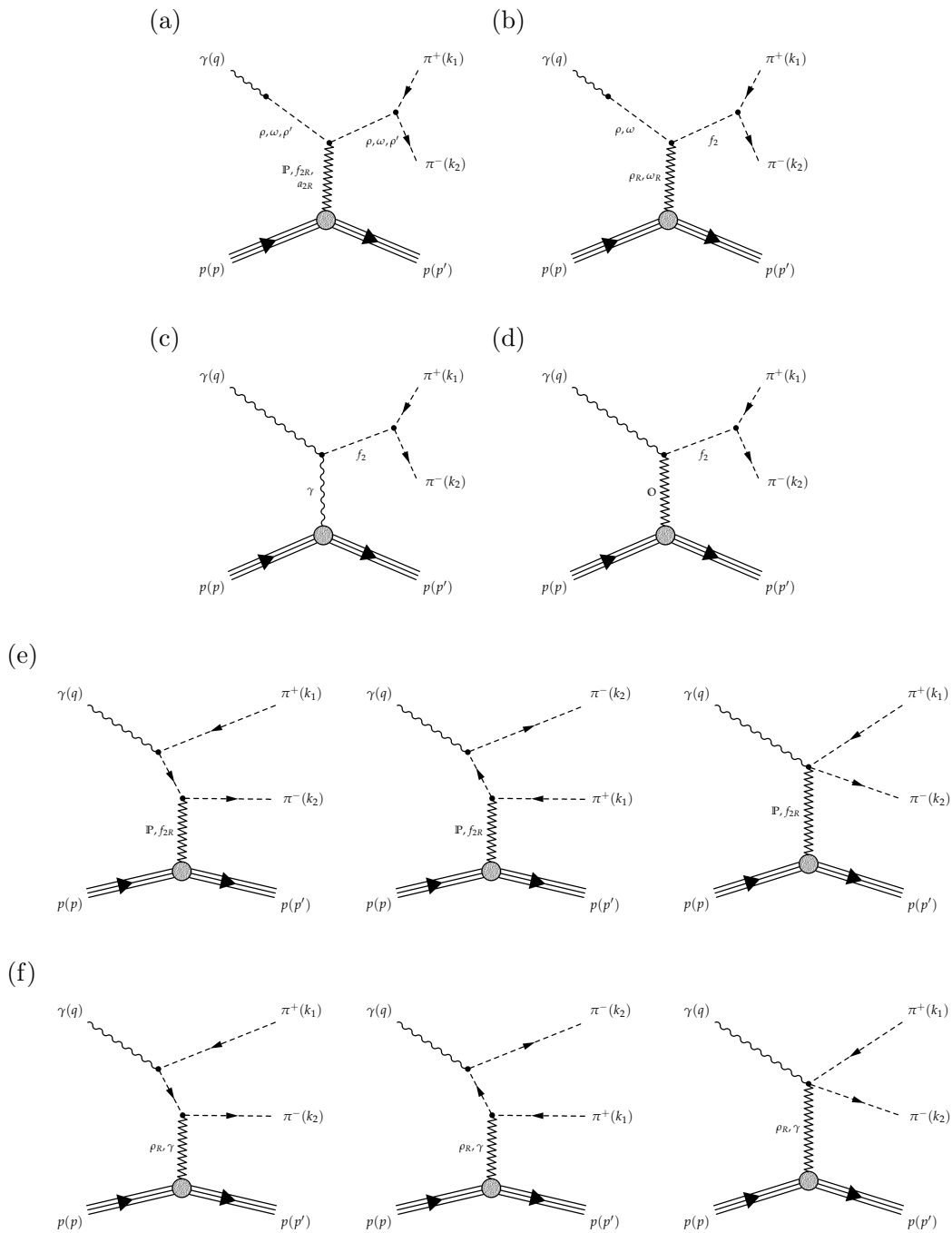
Figure 1. Diagrams for $\pi^+\pi^-$ photoproduction: (a) vector-meson $\rho(770)$, $\omega(782)$, $\rho'(1450)$ production; (b), (c), (d) f_2 production via reggeon, photon (Primakoff effect), and odderon exchanges, respectively; (e) non-resonant $\pi^+\pi^-$ production via pomeron and f_{2R} reggeon exchanges; (f) non-resonant $\pi^+\pi^-$ production via ρ_R and γ exchanges. The diagrams (a) and (e) correspond to $C = +1$ exchange, the diagrams (b), (c), (d), and (f) to $C = -1$ exchange.
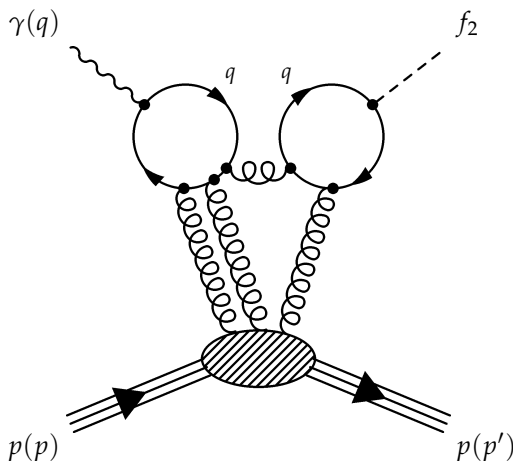
Figure 2. A QCD diagram contributing to f_2 production via odderon exchange.

of π^0 and a_2 mesons on which rather strict experimental limits exist; see [46, 47]. The non-observation of odderon exchange in these reactions was discussed in [48], and it was shown that chiral symmetry implies a strong suppression of π^0 photoproduction via odderon exchange [49].

Note that in figures 1(a), (d), and (e) we include only single-pomeron and single-odderon exchange. The reason is that we consider the pomeron and the odderon as effective exchanges. Alternatively, one could start with a bare pomeron and a bare odderon and then build up a complete reggeon field theory of interacting bare pomerons and bare odderons. That procedure would naturally include pomeron (and odderon) cuts, shadowing effects etc., see for example the discussions in [50–52]. Such a construction is beyond the scope and not in the spirit of our current paper. Instead, we include the effects of multiple pomeron and multiple odderon exchanges in the parameters of the single exchange of an *effective* pomeron or odderon.

Our paper is organised as follows. In section 2 we give analytic expressions for the diagrams of figure 1. In section 3 we present numerical results of total and differential cross sections and discuss the $\pi^+\pi^-$ asymmetries. Section 4 contains our conclusions. Kinematical relations and a list of the effective propagators and vertices are given in appendix A and appendix B, respectively. In appendix C we discuss the behaviour of the differential cross section for $t \to 0$. Appendix D deals with the determination of the Monte Carlo weights for our event generator.

2 Matrix elements, cross sections and asymmetries

We define the matrix element $\mathcal{M}^\mu_{\mathfrak{s}',\mathfrak{s}}$ for the reaction (1.1) as

$$\mathcal{M}^\mu_{\mathfrak{s}',\mathfrak{s}}(k_1, k_2, p', q, p)\epsilon_\mu = \langle \pi^+(k_1), \pi^-(k_2), p(p', \mathfrak{s}') | \mathcal{T} | \gamma(q, \epsilon), p(p, \mathfrak{s}) \rangle . \qquad (2.1)$$

Here k_1, k_2, p', q and p are the four-vectors of the involved particles, ϵ is the photon's polarisation vector, and $\mathfrak{s}$ and $\mathfrak{s}'$ are the spins of the incoming and outgoing proton, respectively. Details of the kinematics of the reaction are discussed in appendix A.

The matrix element (2.1) gets contributions from all diagrams shown in figure 1:

$$\mathcal{M}_{\mathfrak{s}',\mathfrak{s}}^{\mu} = \mathcal{M}_{\mathfrak{s}',\mathfrak{s}}^{(a)\mu} + \mathcal{M}_{\mathfrak{s}',\mathfrak{s}}^{(b)\mu} + \mathcal{M}_{\mathfrak{s}',\mathfrak{s}}^{(c)\mu} + \mathcal{M}_{\mathfrak{s}',\mathfrak{s}}^{(d)\mu} + \mathcal{M}_{\mathfrak{s}',\mathfrak{s}}^{(e)\mu} + \mathcal{M}_{\mathfrak{s}',\mathfrak{s}}^{(f)\mu}\,. \tag{2.2}$$

The diagrams (a) and (e) correspond to $C = +1$ exchange, the diagrams (b), (c), (d) and (f) to $C = -1$ exchange. Gauge invariance requires

$$q_\mu \mathcal{M}_{\mathfrak{s}',\mathfrak{s}}^{\mu} = 0\,. \tag{2.3}$$

In our calculation we find that this gauge-invariance relation holds for each subclass of diagrams (a) to (f) separately:

$$q_\mu \mathcal{M}_{\mathfrak{s}',\mathfrak{s}}^{(a)\mu} = \cdots = q_\mu \mathcal{M}_{\mathfrak{s}',\mathfrak{s}}^{(f)\mu} = 0\,. \tag{2.4}$$

The cross section for (1.1) assuming unpolarised particles in the initial state and no observation of polarisations in the final state reads

$$d\sigma^{\gamma p} = \frac{(2\pi)^4}{2(s-m_p^2)}\left(-\frac{1}{4}\sum_{\mathfrak{s}',\mathfrak{s}}\mathcal{M}_{\mu,\mathfrak{s}',\mathfrak{s}}^* \mathcal{M}_{\mathfrak{s}',\mathfrak{s}}^{\mu}\right)$$
$$\times \frac{1}{(2\pi)^9}\frac{d^3k_1}{2k_1^0}\frac{d^3k_2}{2k_2^0}\frac{d^3p'}{2p'^0}\,\delta^{(4)}(k_1 + k_2 + p' - p - q)\,. \tag{2.5}$$

We define

$$\mathscr{R}\left(s,t,k^2,p\cdot(k_1-k_2),q\cdot(k_1-k_2)\right) = -\frac{1}{4}\sum_{\mathfrak{s}',\mathfrak{s}}\mathcal{M}_{\mu,\mathfrak{s}',\mathfrak{s}}^* \mathcal{M}_{\mathfrak{s}',\mathfrak{s}}^{\mu}\,. \tag{2.6}$$

$\mathscr{R}$ can only depend on the variables indicated, see (A.10), where the Mandelstam variables s and t denote the squared center of mass energy and the squared momentum transfer of the reaction, respectively. The four-vector of the dipion system is defined by the four-vector sum of the π^+ and π^- as $k = k_1 + k_2$.

We can split $\mathscr{R}$ from (2.6) into $\mathscr{R} = \mathscr{R}_+ + \mathscr{R}_-$ where the parts $\mathscr{R}_+$ and $\mathscr{R}_-$ are even and odd, respectively, under the simultaneous sign change of the last two arguments:

$$p\cdot(k_1-k_2) \longrightarrow -p\cdot(k_1-k_2)\,,$$
$$q\cdot(k_1-k_2) \longrightarrow -q\cdot(k_1-k_2)\,. \tag{2.7}$$

$\mathscr{R}_+$ contains the squares of $C = +1$ and $C = -1$ exchange amplitudes, $\mathscr{R}_-$ contains the interference terms of the $C = +1$ and $C = -1$ exchanges. We get

$$\mathscr{R}_+\left(s,t,k^2,p\cdot(k_1-k_2),q\cdot(k_1-k_2)\right)$$
$$= \mathscr{R}_+\left(s,t,k^2,-p\cdot(k_1-k_2),-q\cdot(k_1-k_2)\right)$$
$$= -\frac{1}{4}\sum_{\mathfrak{s}',\mathfrak{s}}\left[\left(\mathcal{M}_{\mu,\mathfrak{s}',\mathfrak{s}}^{(a+e)}\right)^*\mathcal{M}_{\mathfrak{s}',\mathfrak{s}}^{(a+e)\mu} + \left(\mathcal{M}_{\mu,\mathfrak{s}',\mathfrak{s}}^{(b+c+d+f)}\right)^*\mathcal{M}_{\mathfrak{s}',\mathfrak{s}}^{(b+c+d+f)\mu}\right]\,, \tag{2.8}$$

$$\mathscr{R}_- \left(s, t, k^2, p \cdot (k_1 - k_2), q \cdot (k_1 - k_2) \right)$$

$$= -\mathscr{R}_- \left(s, t, k^2, -p \cdot (k_1 - k_2), -q \cdot (k_1 - k_2) \right)$$

$$= -\frac{1}{4} \sum_{\mathfrak{s}', \mathfrak{s}} \left[\left(\mathcal{M}^{(\mathrm{a+e})}_{\mu, \mathfrak{s}', \mathfrak{s}} \right)^* \mathcal{M}^{(\mathrm{b+c+d+f})\mu}_{\mathfrak{s}', \mathfrak{s}} + \left(\mathcal{M}^{(\mathrm{b+c+d+f})}_{\mu, \mathfrak{s}', \mathfrak{s}} \right)^* \mathcal{M}^{(\mathrm{a+e})\mu}_{\mathfrak{s}', \mathfrak{s}} \right]. \qquad (2.9)$$

Observables which are odd under the transformation (2.7) are, therefore, particularly suitable to measure the interference of $C = +1$ and $C = -1$ exchanges, and thus allow to study possible odderon contributions. Examples of such observables are discussed in section 3.

We shall now calculate the amplitudes corresponding to the diagrams of figure 1. The effective propagators and vertices needed for these calculations are mostly taken from [28]. To make the present paper self-contained we list the propagators and vertices needed here in appendix B. We consider it an asset of our approach that given these propagators and vertices we can use the standard rules of QFT to obtain the amplitudes. This guarantees, for instance, that all gauge-invariance and charge-conjugation properties of the amplitudes are automatically satisfied. We shall only present the final results in the following. These explicit expressions are the basis for the construction of our event generator for the reaction (1.1).

2.1 Vector-meson production

Here we discuss the diagrams of figure 1(a), that is, the production of the vector-mesons ρ, ω and ρ' which then decay into $\pi^+ \pi^-$. For ρ and ω we consider both $\mathbb{P}VV$ (pomeron) and $f_{2R}VV$ (reggeon) couplings ($V = \rho, \omega$) whereas for the rather small ρ' contribution only the $\mathbb{P}\rho'\rho'$ coupling is considered. We include strong-isospin violating effects for the (ρ, ω) propagator and for the $\omega \to \pi^+\pi^-$ decay but assume absence of such violations for the couplings of pomeron and reggeons to vector mesons. With the expressions for the propagators, vertices and form factors from appendix B we then obtain

$$\mathcal{M}^{(\mathrm{a})}_{\mu, \mathfrak{s}', \mathfrak{s}} = \sum_{\substack{V=\rho,\omega, \\ V'=\rho,\omega}} \left\{ \mathcal{M}^{(V',V,\mathbb{P})}_{\mu, \mathfrak{s}', \mathfrak{s}} + \mathcal{M}^{(V',V,f_{2R})}_{\mu, \mathfrak{s}', \mathfrak{s}} \right\} + \mathcal{M}^{(a_{2R})}_{\mu, \mathfrak{s}', \mathfrak{s}} + \mathcal{M}^{(\rho',\rho',\mathbb{P})}_{\mu, \mathfrak{s}', \mathfrak{s}}. \qquad (2.10)$$

Here we have for $V', V \in \{\rho, \omega, \rho'\}$

$$\mathcal{M}^{(V',V,\mathbb{P})}_{\mu, \mathfrak{s}', \mathfrak{s}} = \frac{i}{4} e\, s\, F_1(t)\, F_M(t)\, \tilde{F}^{(V)}(k^2)\, g_{V'\pi\pi} \left\{ \mathcal{K}^{(0,V',V)}_{\mu, \mathfrak{s}', \mathfrak{s}} V^{(0,V)}_{\mathbb{P}} - \mathcal{K}^{(2,V',V)}_{\mu, \mathfrak{s}', \mathfrak{s}} V^{(2,V)}_{\mathbb{P}} \right\}, \tag{2.11}$$

$$\mathcal{M}^{(V',V,f_{2R})}_{\mu, \mathfrak{s}', \mathfrak{s}} = \frac{i}{4} e\, s\, F_1(t)\, F_M(t)\, \tilde{F}^{(V)}(k^2)\, g_{V'\pi\pi} \left\{ \mathcal{K}^{(0,V',V)}_{\mu, \mathfrak{s}', \mathfrak{s}} V^{(0,V)}_{f_{2R}} - \mathcal{K}^{(2,V',V)}_{\mu, \mathfrak{s}', \mathfrak{s}} V^{(2,V)}_{f_{2R}} \right\}, \tag{2.12}$$

where for $i = 0, 2$

$$\mathcal{K}^{(i,V',V)}_{\mu, \mathfrak{s}', \mathfrak{s}} = \frac{1}{s^2} (k_1 - k_2)^\nu \Delta^{(V',V)}_T(k^2) \Gamma^{(i)}_{\nu\mu\kappa\lambda}(k, -q)\, \bar{u}_{\mathfrak{s}'}(p') \gamma^\kappa \left(p' + p \right)^\lambda u_{\mathfrak{s}}(p), \qquad (2.13)$$

and

$$V_{\mathbb{P}}^{(0,V)} = \frac{1}{\gamma_V} \, 6 \, \beta_{\mathbb{P}NN} \, a_{\mathbb{P}VV} (-i \, s \, \alpha_{\mathbb{P}}')^{\alpha_{\mathbb{P}}(t)-1} \, ,$$

$$V_{\mathbb{P}}^{(2,V)} = \frac{1}{\gamma_V} \, 3 \, \beta_{\mathbb{P}NN} \, b_{\mathbb{P}VV} (-i \, s \, \alpha_{\mathbb{P}}')^{\alpha_{\mathbb{P}}(t)-1} \, , \tag{2.14}$$

$$V_{f_{2R}}^{(0,V)} = \frac{1}{\gamma_V} \frac{2 \, g_{f_{2R}pp}}{M_0} \, a_{f_{2R}VV} (-i \, s \, \alpha_{\mathbb{R}_+}')^{\alpha_{\mathbb{R}_+}(t)-1} \, ,$$

$$V_{f_{2R}}^{(2,V)} = \frac{1}{\gamma_V} \frac{g_{f_{2R}pp}}{M_0} \, b_{f_{2R}VV} (-i \, s \, \alpha_{\mathbb{R}_+}')^{\alpha_{\mathbb{R}_+}(t)-1} \, . \tag{2.15}$$

For a_{2R} reggeon exchange in figure 1(a) we have four contributions. The photon can turn into a ρ which, upon a_{2R} exchange, turns into a ω; and we can have the rôles of ρ and ω exchanged. Both, the final ω and ρ, can then, by propagator mixing, go to $V' \in \{\rho, \omega\}$ which decays to $\pi^+\pi^-$. The amplitude taking into account all these processes is

$$\mathcal{M}_{\mu,\mathfrak{s}',\mathfrak{s}}^{(a_{2R})} = \frac{i}{4} \, e \, s \, F_1(t) \, F_M(t) \, \tilde{F}^{(\rho)}(k^2) \frac{g_{a_{2R}pp}}{M_0} \, (-i \, s \, \alpha_{\mathbb{R}_+}')^{\alpha_{\mathbb{R}_+}(t)-1}$$

$$\times \sum_{V'=\rho,\omega} g_{V'\pi\pi} \left\{ \left[\mathcal{K}_{\mu,\mathfrak{s}',\mathfrak{s}}^{(0,V',\omega)} \frac{1}{\gamma_\rho} + \mathcal{K}_{\mu,\mathfrak{s}',\mathfrak{s}}^{(0,V',\rho)} \frac{1}{\gamma_\omega} \right] 2 a_{a_{2R}\omega\rho} \right.$$

$$\left. - \left[\mathcal{K}_{\mu,\mathfrak{s}',\mathfrak{s}}^{(2,V',\omega)} \frac{1}{\gamma_\rho} + \mathcal{K}_{\mu,\mathfrak{s}',\mathfrak{s}}^{(2,V',\rho)} \frac{1}{\gamma_\omega} \right] b_{a_{2R}\omega\rho} \right\} \, . \tag{2.16}$$

Here and in the following $M_0 = 1 \, \text{GeV}$ is used in various places for dimensional reasons. All quantities occurring here and their definitions can be found in table 1 of appendix B.

We note that for the ρ' meson, apart from the known mass $m_{\rho'}$ and the width $\Gamma_{\rho'}$, only the combinations

$$g_{\rho'\pi\pi} \frac{1}{\gamma_{\rho'}} a_{\mathbb{P}\rho'\rho'} \qquad \text{and} \qquad g_{\rho'\pi\pi} \frac{1}{\gamma_{\rho'}} b_{\mathbb{P}\rho'\rho'} \tag{2.17}$$

enter in the expression (2.10) for $\mathcal{M}_{\mu,\mathfrak{s}',\mathfrak{s}}^{(a)}$. Thus, only these two combinations can be determined by studying the ρ' contribution to the reaction (1.1).

2.2 Production of f_2 by reggeon exchange

Here the corresponding diagram is shown in figure 1(b). We get with the expressions for the propagators and vertices from appendix B

$$\mathcal{M}_{\mu,\mathfrak{s}',\mathfrak{s}}^{(b)} = \frac{1}{4} \, e \, s \, F_1(t) \, F_M(t) \left[F^{(f_2\pi\pi)}(k^2) \right]^2 g_{f_2\pi\pi} \sum_{V=\rho,\omega} \left\{ \mathcal{N}_{\mu,\mathfrak{s}',\mathfrak{s}}^{(0)} W_V^{(0)} - \mathcal{N}_{\mu,\mathfrak{s}',\mathfrak{s}}^{(2)} W_V^{(2)} \right\} \, . \tag{2.18}$$

We find for $i = 0, 2$

$$\mathcal{N}_{\mu,\mathfrak{s}',\mathfrak{s}}^{(i)} = \frac{2}{s} \left[(k_1 - k_2)^\kappa \, (k_1 - k_2)^\lambda - \frac{1}{4} g^{\kappa\lambda} \, (k_1 - k_2)^2 \right]$$

$$\times \Delta_{\kappa\lambda}^{(f_2)\kappa'\lambda'}(k) \, \Gamma_{\mu\nu\kappa'\lambda'}^{(i)}(q, p-p') \, \bar{u}_{\mathfrak{s}'}(p')\gamma^\nu u_{\mathfrak{s}}(p) \, , \tag{2.19}$$

and for $V = \rho, \omega$

$$W_V^{(0)} = \frac{1}{\gamma_V} \frac{1}{M_0} \frac{1}{M_-^2} \, g_{V_R pp} \, 2 \, a_{V_R V f_2} (-\, i \, s \, \alpha'_{\mathbb{R}_-})^{\alpha_{\mathbb{R}_-}(t)-1} \, ,$$

$$W_V^{(2)} = \frac{1}{\gamma_V} \frac{1}{M_0} \frac{1}{M_-^2} \, g_{V_R pp} \, b_{V_R V f_2} (-\, i \, s \, \alpha'_{\mathbb{R}_-})^{\alpha_{\mathbb{R}_-}(t)-1} \, . \tag{2.20}$$

For the definition of the parameters occurring here we refer again to table 1 in appendix B.

2.3 Production of f_2 by photon exchange

Here we calculate the amplitude corresponding to the diagram of figure 1(c). Using the expressions for the propagators and vertices from appendix B we get the following:

$$\mathcal{M}_{\mu,\mathfrak{s}',\mathfrak{s}}^{(c)} = \frac{1}{4} \, e \, s \, g_{f_2\pi\pi} \, F_M(t) \left[F^{(f_2\pi\pi)}(k^2) \right]^2$$

$$\times \left\{ F_1(t) \left[\mathcal{N}_{\mu,\mathfrak{s}',\mathfrak{s}}^{(0)} W_\gamma^{(0)} - \mathcal{N}_{\mu,\mathfrak{s}',\mathfrak{s}}^{(2)} W_\gamma^{(2)} \right] + F_2(t) \left[S_{\mu,\mathfrak{s}',\mathfrak{s}}^{(0)} W_\gamma^{(0)} - S_{\mu,\mathfrak{s}',\mathfrak{s}}^{(2)} W_\gamma^{(2)} \right] \right\} \, . \tag{2.21}$$

Here the $\mathcal{N}_{\mu,\mathfrak{s}',\mathfrak{s}}^{(i)}$ $(i = 0, 2)$ are taken from (2.19) and we have defined for $i = 0, 2$:

$$S_{\mu,\mathfrak{s}',\mathfrak{s}}^{(i)} = \frac{2}{s} \left[(k_1 - k_2)^\kappa (k_1 - k_2)^\lambda - \frac{1}{4} g^{\kappa\lambda} (k_1 - k_2)^2 \right]$$

$$\times \Delta_{\kappa\lambda}^{(f_2)\kappa'\lambda'}(k) \, \Gamma_{\mu\nu\kappa'\lambda'}^{(i)}(q, p - p') \, \bar{u}_{\mathfrak{s}'}(p') \frac{i}{2m_p} \sigma^{\nu\nu'}(p' - p)_{\nu'} u_{\mathfrak{s}}(p) \, , \tag{2.22}$$

and

$$W_\gamma^{(0)} = - \frac{1}{M_0} \frac{1}{t} 2 \, a_{f_2\gamma\gamma} \, ,$$

$$W_\gamma^{(2)} = - \frac{1}{M_0} \frac{1}{t} b_{f_2\gamma\gamma} \, . \tag{2.23}$$

2.4 Production of f_2 by odderon exchange

Now we come to the diagram of figure 1(d) describing f_2 production via odderon exchange. We get here, using the formulae from appendix B,

$$\mathcal{M}_{\mu,\mathfrak{s}',\mathfrak{s}}^{(d)} = \frac{1}{4} \, e \, s \, g_{f_2\pi\pi} \, F_1(t) \, F_M(t) \left[F^{(f_2\pi\pi)}(k^2) \right]^2 \left[\mathcal{N}_{\mu,\mathfrak{s}',\mathfrak{s}}^{(0)} W_{\mathbb{O}}^{(0)} - \mathcal{N}_{\mu,\mathfrak{s}',\mathfrak{s}}^{(2)} W_{\mathbb{O}}^{(2)} \right] \, . \tag{2.24}$$

Here again the $\mathcal{N}_{\mu,\mathfrak{s}',\mathfrak{s}}^{(i)}$ $(i = 0, 2)$ are as in (2.19) and we have

$$W_{\mathbb{O}}^{(0)} = - \frac{1}{M_0^2} 3 \, \beta_{\mathbb{O}pp} \, \eta_{\mathbb{O}} \, 2 \, \hat{a}_{\mathbb{O}\gamma f_2} (-\, i \, s \, \alpha'_{\mathbb{O}})^{\alpha_{\mathbb{O}}(t)-1} \, ,$$

$$W_{\mathbb{O}}^{(2)} = - \frac{1}{M_0^2} 3 \, \beta_{\mathbb{O}pp} \, \eta_{\mathbb{O}} \, \hat{b}_{\mathbb{O}\gamma f_2} (-\, i \, s \, \alpha'_{\mathbb{O}})^{\alpha_{\mathbb{O}}(t)-1} \, . \tag{2.25}$$

2.5 Non-resonant production of $\pi^+\pi^-$ by pomeron and f_{2R} exchange

The diagrams of figure 1(e) describe the non-resonant production of a $\pi^+\pi^-$ pair by exchange of the pomeron $\mathbb{P}$ and the f_{2R}. This type of process was first discussed by Söding [53] following a suggestion by Drell [54, 55]. However, typically it is difficult to maintain gauge invariance in calculations of this Drell-Söding term.

In our approach the effective vertices are derived from coupling Lagrangians. In this formalism we include the coupling to photons by the minimal substitution rule, i. e. derivatives are replaced by corresponding covariant derivatives. Thereby we are guaranteed to have gauge invariance automatically. For the pomeron exchange contribution to non-resonant $\pi^+\pi^-$ production we start from the $\mathbb{P}\pi\pi$ Lagrangian in equation (7.3) of [28]. We note that for writing down such a $\mathbb{P}\pi\pi$ Lagrangian it is essential to consider the pomeron exchange as an effective tensor exchange. The minimal substitution gives then the Lagrangian (B.66) which fixes the $\mathbb{P}\gamma\pi^+\pi^-$ contact term in figure 1(e). Using analogous arguments the $f_{2R}\gamma\pi^+\pi^-$ contact term in figure 1(e) is fixed. With the formulae of appendix B we obtain

$$
\begin{aligned}
\mathcal{M}^{(e)}_{\mu,\mathfrak{s}',\mathfrak{s}} = {} & \frac{i}{2}\,\frac{1}{s}\,e\,F_1(t)\,F_M(t) \\
& \times \left[6\,\beta_{\mathbb{P}NN}\,\beta_{\mathbb{P}\pi\pi}(-i\,s\,\alpha'_{\mathbb{P}})^{\alpha_{\mathbb{P}}(t)-1} + \frac{1}{2M_0^2}\,g_{f_{2R}pp}\,g_{f_{2R}\pi\pi}(-i\,s\,\alpha'_{\mathbb{R}_+})^{\alpha_{\mathbb{R}_+}(t)-1} \right] \\
& \times \left\{ -\frac{1}{(q-k_1)^2-m_\pi^2}\,(q-2k_1)_\mu\,(q-k_1+k_2)_\kappa\,(q-k_1+k_2)_\lambda \right. \\
& \qquad + \frac{1}{(q-k_2)^2-m_\pi^2}\,(q-2k_2)_\mu\,(q+k_1-k_2)_\kappa\,(q+k_1-k_2)_\lambda \\
& \qquad \left. + 2\,g_{\mu\kappa}\,(k_2-k_1)_\lambda + 2\,g_{\mu\lambda}\,(k_2-k_1)_\kappa \right\} \\
& \times \bar{u}_{\mathfrak{s}'}(p')\left[\frac{1}{2}\,\gamma^\kappa\,(p'+p)^\lambda + \frac{1}{2}\,\gamma^\lambda\,(p'+p)^\kappa - \frac{1}{4}\,g^{\kappa\lambda}\,(p\!\!\!/'+p\!\!\!/) \right]u_{\mathfrak{s}}(p)\,. \quad (2.26)
\end{aligned}
$$

Note that all three diagrams in figure 1(e) come with the same energy dependence, that is with the same energy variable s in the Regge factor. In Regge language this corresponds to saying that the propagation of the pion between its couplings to the photon and to the pomeron or f_{2R} in the first two diagrams of figure 1(e) is part of the impact factor. This ensures the gauge invariance of the expression (2.26) and is in agreement with Regge factorisation. Due to its lower spin the t-channel propagation of the pion over a sizeable range in rapidity is strongly suppressed with respect to pomeron and f_{2R} exchange.

2.6 Non-resonant production of $\pi^+\pi^-$ by ρ_R and photon exchange

From the diagrams of figure 1(f) we get the following amplitude for non-resonant $\pi^+\pi^-$ production via ρ_R and photon exchange:

$$
\begin{aligned}
\mathcal{M}^{(f)}_{\mu,\mathfrak{s}',\mathfrak{s}} = {} & -\frac{1}{2}e\,F_1(t)\,F_M(t)\frac{1}{M_-^2}\,g_{\rho_R\pi\pi}\,g_{\rho_Rpp}(-i\,s\,\alpha'_{\mathbb{R}_-})^{\alpha_{\mathbb{R}_-}(t)-1} \\
& \times \left\{ \frac{1}{(q-k_1)^2-m_\pi^2}\,(q-2k_1)_\mu\,(q-k_1+k_2)_\nu \right.
\end{aligned}
$$

$$+ \frac{1}{(q-k_2)^2 - m_\pi^2} (q-2k_2)_\mu (q+k_1-k_2)_\nu - 2\, g_{\mu\nu} \Big\} \bar{u}_{\mathfrak{s}'}(p')\, \gamma^\nu u_{\mathfrak{s}}(p)$$

$$+ e^3 \frac{1}{t} \left\{ \frac{1}{(q-k_1)^2 - m_\pi^2} (q-2k_1)_\mu (q-k_1+k_2)_\nu \right.$$

$$\left. + \frac{1}{(q-k_2)^2 - m_\pi^2} (q-2k_2)_\mu (q+k_1-k_2)_\nu - 2\, g_{\mu\nu} \right\}$$

$$\times \bar{u}_{\mathfrak{s}'}(p') \left[\gamma^\nu\, F_1(t) + \frac{i}{2m_p} \sigma^{\nu\lambda} \left(p'-p\right)_\lambda\, F_2(t) \right] u_{\mathfrak{s}}(p)\,. \tag{2.27}$$

As it must be, the amplitudes corresponding to $C = +1$ exchanges are odd under the exchange of the pion momenta, $k_1 \leftrightarrow k_2$; see (2.10)–(2.16) and (2.26). The amplitudes with $C = -1$ exchanges are even under $k_1 \leftrightarrow k_2$; see (2.18), (2.19), (2.21), (2.22), (2.23) and (2.27). From these properties follow the symmetry relations for $\mathscr{R}_+$ and $\mathscr{R}_-$ in (2.8) and (2.9), respectively.

In agreement with Regge factorisation the energy dependence of all three diagrams of figure 1(f) is the same. This is analogous to the case of pomeron and f_{2R} exchange, see section 2.5.

The question may be raised whether we should have included more diagrams than those of figure 1 in our calculations. For instance, one may think of diagrams as the first two in figure 1(e) where the internal pion line is replaced by the exchange of a heavy meson like $a_1(1260)$, $a_2(1320)$, or $\pi(1300)$. We think that this would not be appropriate. Our model assumes that these mesonic degrees of freedom are integrated out in the functional integral. Let us take, as an example, a_1 exchange in diagrams of the type of figure 1(e). This would assume a direct $\gamma\pi a_1$ coupling — which would probably present some problems with gauge invariance. Even assuming these problems to be solved we would get essentially a $\mathbb{P}\gamma\pi\pi$ contact term from such a heavy meson exchange. Thus, in this case, the effect of a_1 exchange should contribute and should be effectively already included in the third diagram of figure 1(e). More generally, such heavy meson exchanges would contribute to so-called "internal form factors" for the Drell-Söding contribution. Such form factors will be discussed in [56]. But maybe it is more resaonable to assume that the photon couples to πa_1 via an intermediate ρ. Then the first two diagrams of figure 1(e) with the photon first converting to ρ which then couples to πa_1 are really part of the diagram of figure 1(a) with the a_1 exchange contributing to the form factors $\tilde{F}^\rho$ in the $\mathbb{P}\rho\rho$ vertex (B.82). To conclude: it is part of our model assumptions that the effects of the heavy mesons mentioned above are included in the contact terms and form factors of our vertices. Of course, this assumption is subject to an experimental check.

This concludes our presentation of the amplitudes corresponding to the diagrams of figure 1(a-f). For further analysis an event generator is built, based on the following techniques. For the evaluation of the matrix elements the FeynCalc package [57] (version 8.2.0) is used and the results are cross-checked with a direct implementation based on the template-library LTensor [58]. Based on that, a weight and the kinematic variables of an event are determined using a standard Monte Carlo (MC) method with pre-sampling, see appendix D. The output of the event generator is stored in a standard format of the

ROOT-package [59] and used to derive (partially integrated) differential cross sections as a function of various variables.

3 Results

In this section we present selected results for cross sections, angular distributions and asymmetries. For the numerical evaluation of the formulae presented above we use a set of default parameters for the model [28]. These default parameters are given in table 1 of appendix B. Many of the parameters are well constrained while we can only guess the values of some others. In the present study we do not make any attempt to fit the parameters to data. That would be desirable in general but is not the scope of the present paper. Instead, we concentrate here on studying the qualitative features of the reaction (1.1) in the model. We find that some asymmetries seem particularly promising for detailed experimental studies as they allow to enhance interesting effects by choosing suitable cuts on the data. In particular, we point out promising ways to look for effects of the elusive odderon.

3.1 Cross sections

We start with the total cross section for the reaction (1.1) which we integrate here from the dipion mass threshold to $1.5\,\mathrm{GeV}$ (as is done for example in the experimental study [18]):

$$\sigma\left(\gamma p \to \pi^+\pi^- p\right) \quad \text{for } 2m_\pi < m_{\pi^+\pi^-} < 1.5\,\mathrm{GeV} \quad \text{and} \ -1\,\mathrm{GeV}^2 \le t \le 0\,. \tag{3.1}$$

In figure 3 we show the cross section as function of $W_{\gamma p}$. Also the cross sections for various subclasses of diagrams according to figure 1 are shown. The dominant contribution to the total cross section comes from ρ^0 production. Total cross section data for $\gamma p \to \rho^0 p$ are shown for illustration. They are taken from figure 10 of [18] and are defined in the same mass range as given in (3.1). For $W_{\gamma p} \gtrsim 5\,\mathrm{GeV}$ our model describes the essential features of the data. At very low $W_{\gamma p}$-values an agreement with data is not expected as further processes, not included in our high-energy model, contribute to the cross section. We emphasise again that our model curves are just examples and not fits. Note that our model contains all contributions to the reaction (1.1) given by the diagrams of figure 1, not just the ρ contribution, which nonetheless dominates the total cross section.

As a second example we show in figure 4 the differential cross section $d\sigma/dt\,(\gamma p \to \pi^+\pi^- p)$ as function of $|t|$. We integrate over $m_{\pi^+\pi^-}$ as indicated in (3.1) and choose $W_{\gamma p} = 30\,\mathrm{GeV}$. Again, in addition to the full differential cross section also the various contributions from individual subprocesses are shown. The production of ρ mesons is dominant for all values of t, followed by non-resonant $\pi^+\pi^-$ production and the — by more than three orders of magnitude — smaller f_2 production. The cross section of all contributions falls approximately exponentially as function of $|t|$ for $|t| \gtrsim 0.1\,\mathrm{GeV}^2$. We note that the Primakoff contribution to f_2 production, figure 1(c), has a singularity for $|t| \to 0$. This singularity is, of course, never reached since for reaction (1.1) there is a minimal value for $|t|$, $|t_{\min}| > 0$ (see (A.12)). The singularity is driven by the photon propagator and behaves as $1/|t|$. In contrast, the reggeon contributions from ρ_R, ω_R and
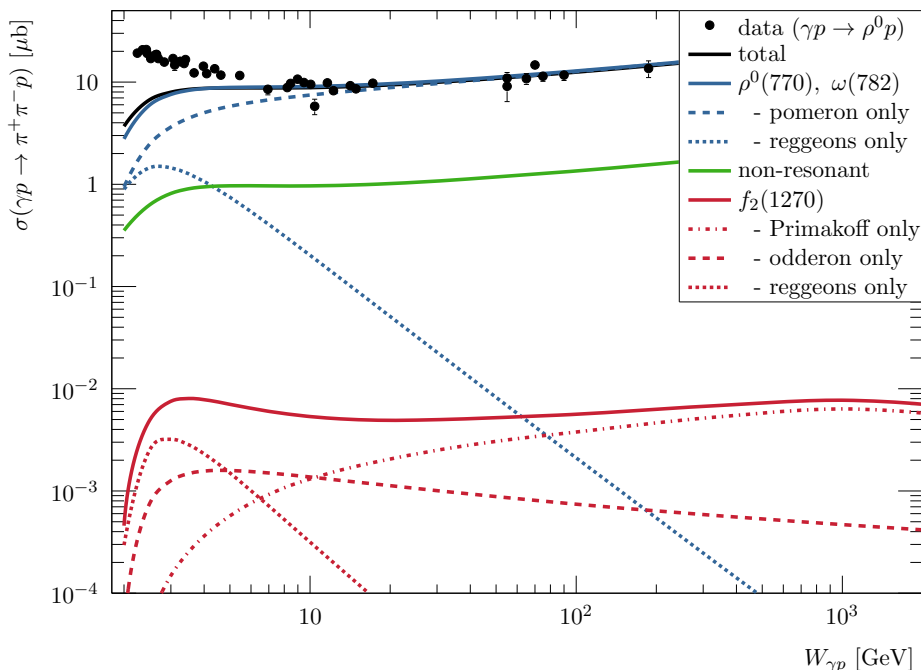
Figure 3. The total cross section $\sigma\left(\gamma p \rightarrow \pi^+ \pi^- p\right)$ as a function of the center-of-mass energy $W_{\gamma p}$. The cross section is integrated over $2m_\pi \leq m_{\pi^+ \pi^-} \leq 1.5\,\mathrm{GeV}$ and $-1\,\mathrm{GeV}^2 \leq t \leq 0$. The full model and individual contributions from vector meson production, non-resonant processes, and f_2 production are shown. The reggeon contributions comprise f_{2R} and a_{2R} in case of vector meson, and ρ_R and ω_R in case of f_2 production. High energy data for $\sigma\left(\gamma p \rightarrow \rho^0 p\right)$ from H1 [17] and ZEUS [16, 18] at HERA as well as fixed target data, referenced in [18], are shown for illustration.

odderon exchange, figures 1(b) and 1(d), show a dip for $|t| \rightarrow 0$. An explanation for this different behaviour is given in appendix C.

Also note that with the chosen default parameters odderon exchange is the dominant contribution to f_2 production for $|t| \gtrsim 0.1\,\mathrm{GeV}^2$ which can be exploited in an experimental search to enhance a possible odderon signal. Reggeon contributions to f_2 production are negligible at $W_{\gamma p} = 30\,\mathrm{GeV}$ or higher values.

In figure 5 we show the differential cross section $d\sigma/dm_{\pi^+\pi^-}\left(\gamma p \rightarrow \pi^+ \pi^- p\right)$ as function of the $\pi^+\pi^-$ invariant mass $m_{\pi^+\pi^-}$ for the range from threshold to $m_{\pi^+\pi^-} = 2\,\mathrm{GeV}$, and enlarged for the ρ mass region. The differential cross sections are shown for $W_{\gamma p} = 30\,\mathrm{GeV}$ integrated in the range $-1\,\mathrm{GeV}^2 \leq t \leq 0$. The contributions of various subclasses of diagrams are also shown as well as the dominant contributions from interferences in the ρ mass region. The resonance structure of the ρ peak is clearly visible. Note that the shape of the $\rho(770)$ peak from the diagrams of figure 1(a) alone is rather symmetric. The skewing of the ρ shape caused by the interference of the diagrams of figures 1(a) and 1(e),(f) (non-resonant contributions) is clearly exposed. We see here the Drell-Söding mechanism [53–55] at work. Note that the skewing depends crucially on the choice of the ρ form factor parameterisation, which was here implemented according to equation (B.85). Furthermore, the effect of the ρ–ω interference, the steep falloff at the top of the ρ^0 peak, is clearly visible.
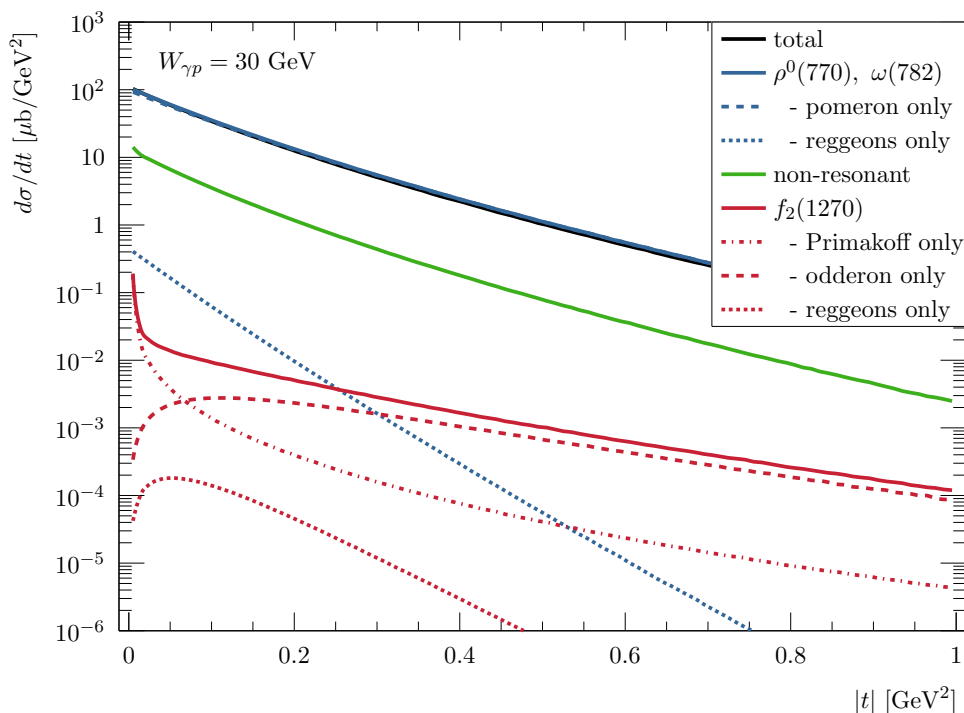
Figure 4. The differential cross section $d\sigma/dt\,(\gamma p \to \pi^+\pi^- p)$ as function of $|t|$. The cross section is integrated over the range $2m_\pi \le m_{\pi^+\pi^-} \le 1.5\,\text{GeV}$ and given for fixed $W_{\gamma p} = 30\,\text{GeV}$. In addition to the full model results also contributions from the main diagrams are shown, see figure 3 for explanations.
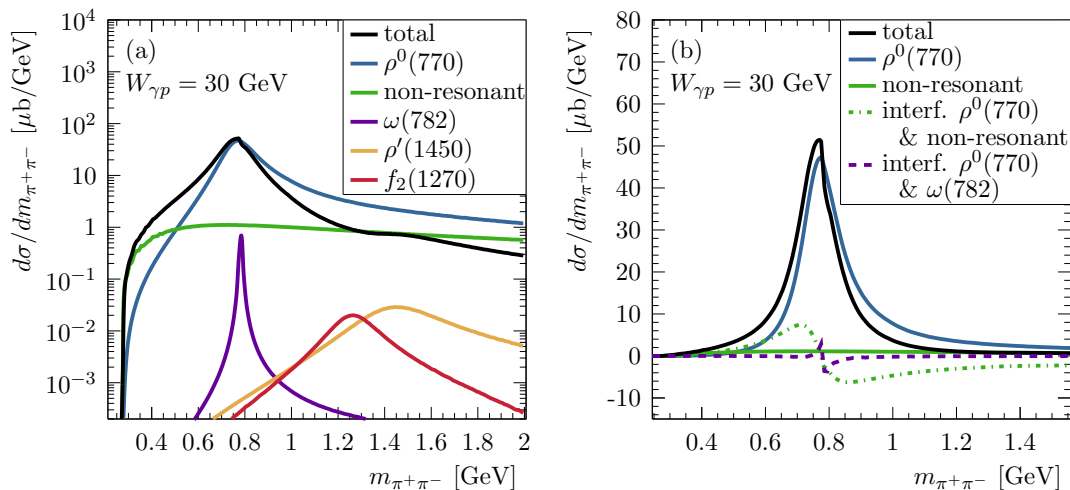

Figure 5. Differential cross sections $d\sigma/dm_{\pi^+\pi^-}\,(\gamma p \to \pi^+\pi^- p)$ as function of $m_{\pi^+\pi^-}$ for fixed $W_{\gamma p} = 30\,\text{GeV}$ and integrated over the range $-1\,\text{GeV}^2 \le t \le 0$. (a) The full model, non-resonant contributions and the contributions from the resonances $\rho^0(770)$, $\omega(782)$, $f_2(1270)$ and $\rho'(1450)$ are shown. (b) Dominant contributions in the ρ mass region including the leading interferences of $\rho^0(770)$ with the non-resonant $\pi^+\pi^-$ production and the $\omega(782)$ meson are shown.

In the mass region of the ρ' meson, $1.2\,\text{GeV} \lesssim m_{\pi^+\pi^-} \lesssim 1.6\,\text{GeV}$, a distortion of the skewed ρ line-shape due to the interference of the ρ' diagram in figure 1(a), and to a lesser extent the f_2 diagrams in figures 1(b, c, d), with the ρ meson and the non-resonant contribution is visible. However, clear resonance peaks in the $m_{\pi^+\pi^-}$ distribution due to f_2 and ρ' do not show up for the chosen default parameters.

3.2 Angular distributions

In the following we study the pion angular distribution in the $\pi^+\pi^-$ rest system. For illustration we choose as reference system here the proton-Jackson system, see figure 10 in appendix A, in which the polar angle $\theta_{k_1,p}$ of the π^+ is measured with respect to the incoming proton direction. This and other reference systems are discussed in detail in appendix A. As the decay-angle distribution is mass dependent and mainly driven by the spin of the resonance in case of decays we study the angular distribution in the ρ and the f_2 mass regions separately.

In figure 6(a) the differential distribution $d\sigma/d\cos\theta_{k_1,p}\,(\gamma p \to \pi^+\pi^- p)$ in the ρ mass region, $0.45\,\text{GeV} \leq m_{\pi^+\pi^-} \leq 1.1\,\text{GeV}$, is shown as function of $\cos\theta_{k_1,p}$. The distribution shows a typical $\propto \sin^2\theta_{k_1,p}$ behaviour as is expected for photo-produced vector mesons if (approximate) s-channel helicity conservation [60] holds.[1] (For the general formalism of helicity amplitudes in this context see [61, 62].)

In figure 6(b) the same distribution is shown in the f_2 mass region $1.1\,\text{GeV} \leq m_{\pi^+\pi^-} \leq 1.35\,\text{GeV}$. In addition to the dominant ρ contribution, which exhibits again the typical $\propto \sin^2\theta_{k_1,p}$ behaviour, the small f_2 contributions show more features in the angular distribution as it is expected for a $J = 2$ resonance. The interference of the C-even and C-odd exchange contributions leads to a small asymmetry of the $\cos\theta_{k_1,p}$ distribution as shown in figure 6(c). This asymmetry comes dominantly from the interference between the ρ and f_2 production diagrams. The asymmetry is partially cancelled by the interference of the f_2 resonance with non-resonant $\pi^+\pi^-$ production but a net asymmetry remains if all diagrams are included. The resulting charge asymmetries are discussed in more detail in the following.

3.3 Charge asymmetries

Let us now turn to asymmetries in the $\pi^+\pi^-$ rest system. As already noted in section 2 the interference of diagrams with exchange of $C = +1$ and $C = -1$ objects is signalled by an asymmetry under

$$\mathbf{k}_1 \to -\mathbf{k}_1 \, ; \tag{3.2}$$

see the discussion following (2.7) and (2.27).

We note first that P-invariance tells us that the distributions of the π^+ momentum must be symmetric under a reflection on the reaction plane, which in the $\pi^+\pi^-$ system is given by the plane spanned by the momenta of the incoming proton and the outgoing

---

[1]Strictly speaking, s-channel helicity conservation should be discussed in the helicity system (see appendix A) which for small t is very close to the proton-Jackson system.
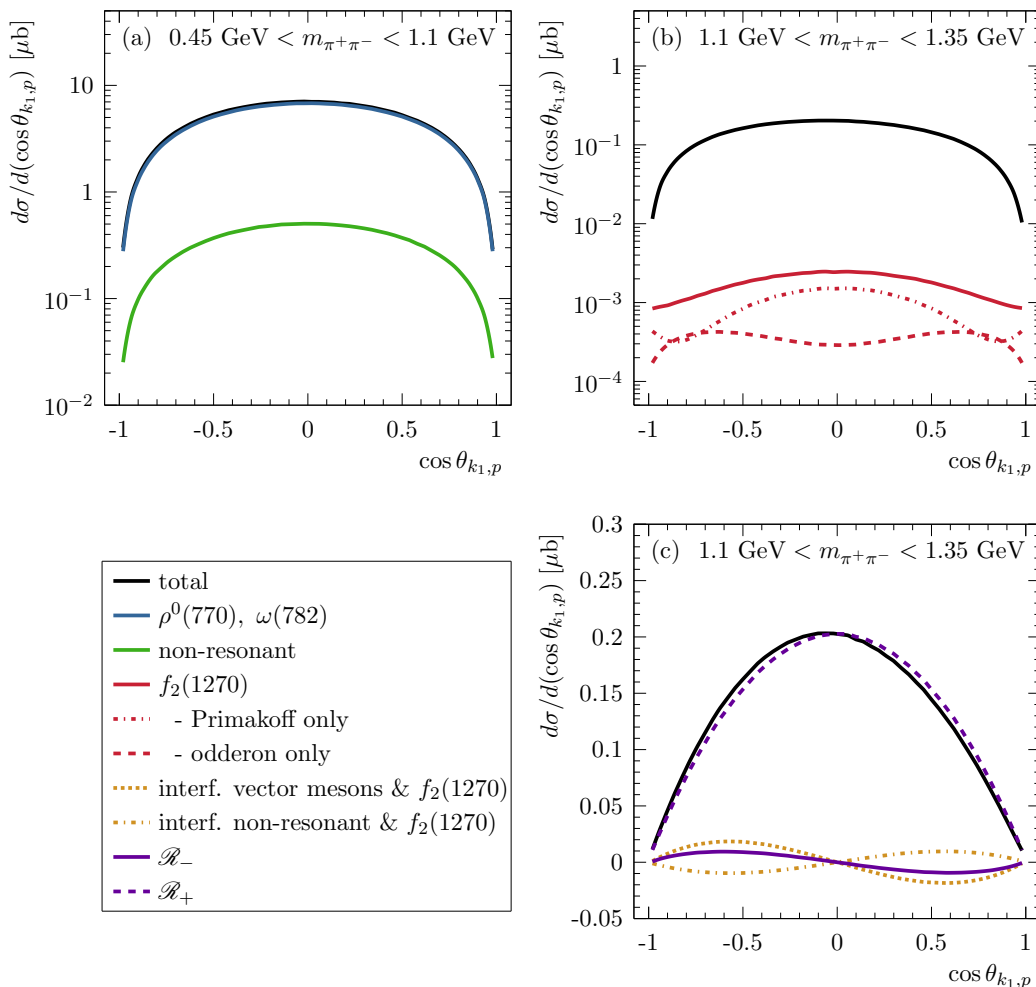
Figure 6. Differential cross section $d\sigma/d\cos\theta_{k_1,p}$ $(\gamma p \to \pi^+\pi^- p)$ as function of the cosine of the polar angle $\theta_{k_1,p}$ in the proton-Jackson system for fixed $W_{\gamma p} = 30\,\text{GeV}$ and integrated over the range $-1\,\text{GeV}^2 \leq t \leq 0$. The full model and the dominant contributions for the mass regions $0.45\,\text{GeV} \leq m_{\pi^+\pi^-} \leq 1.1\,\text{GeV}$ (ρ mass region) and $1.1\,\text{GeV} \leq m_{\pi^+\pi^-} \leq 1.35\,\text{GeV}$ (f_2 mass region) are shown in (a) and (b),(c), respectively. (c) shows in addition to the full differential cross section the dominant interference terms on a linear scale. All contributions are explained in the legend; for $\mathscr{R}_+$ and $\mathscr{R}_-$ see (2.8) and (2.9).

proton. We turn, therefore, to charge asymmetries which are defined with respect to specific directions (axes) in the reaction plane. In the literature many different definitions of reference systems can be found, which are used to study asymmetries. A summary of the different definitions is given in appendix A.

We start our discussion of charge asymmetries in the proton-Jackson system, for which the $\theta_{k_1,p}$ distributions were shown in the previous section. It is convenient to define a $\theta_{k_1,p}$ dependent charge asymmetry:

$$\widehat{\mathcal{A}}(\cos\theta_{k_1,p}) = \frac{\frac{d\sigma}{d\cos\theta_{k_1,p}}(\cos\theta_{k_1,p}) - \frac{d\sigma}{d\cos\theta_{k_1,p}}(-\cos\theta_{k_1,p})}{\frac{d\sigma}{d\cos\theta_{k_1,p}}(\cos\theta_{k_1,p}) + \frac{d\sigma}{d\cos\theta_{k_1,p}}(-\cos\theta_{k_1,p})} \qquad \text{for} \ \cos\theta_{k_1,p} > 0\,. \qquad (3.3)$$
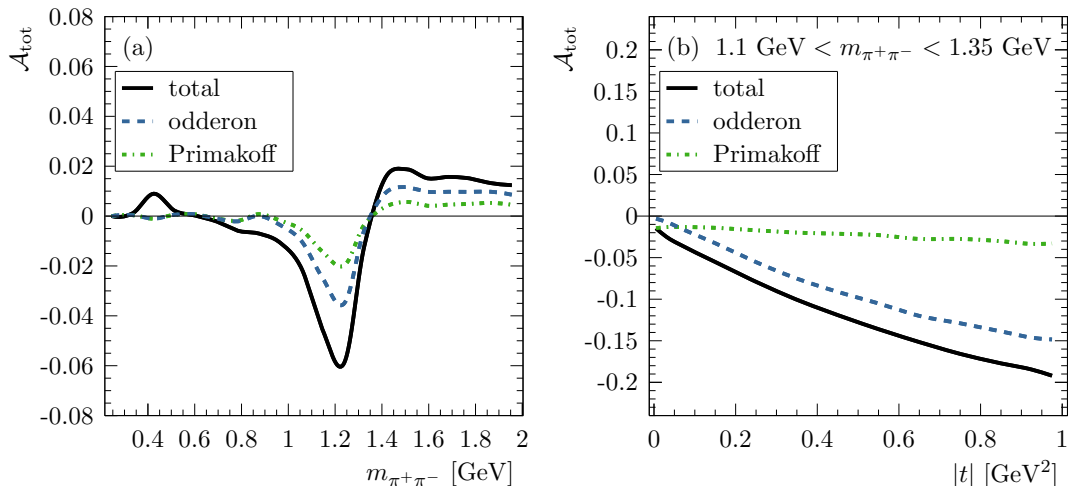
Figure 7. Total charge asymmetry $\mathcal{A}_{\text{tot}}$ (3.4) in the proton-Jackson system as function of the (a) invariant mass of the $\pi^+\pi^-$ system and (b) squared momentum transfer t. The asymmetries are presented for fixed $W_{\gamma p} = 30\,\text{GeV}$ and (a) integrated over the range $-1\,\text{GeV}^2 \leq t \leq 0$ and (b) integrated over the range $1.1\,\text{GeV} < m_{\pi^+\pi^-} < 1.35\,\text{GeV}$. The individual contributions to the asymmetries from photon (Primakoff) and odderon exchange are shown by the green dashed-dotted and blue dashed lines, respectively.

We also define a total charge asymmetry:

$$\mathcal{A}_{\text{tot}} = \frac{\sigma_+ - \sigma_-}{\sigma_+ + \sigma_-}\,, \tag{3.4}$$

using the definitions

$$\sigma_\pm = \int_0^1 \frac{d\sigma}{d\cos\theta_{k_1,p}} \left(\pm\cos\theta_{k_1,p}\right) d\cos\theta_{k_1,p}\,. \tag{3.5}$$

In figure 7(a) the total charge asymmetry defined in the proton-Jackson system is shown as function of the invariant mass of the $\pi^+\pi^-$ system. A negative asymmetry of a few percent is visible in the f_2 resonance region for the chosen parameter values. This asymmetry is mainly due to the interference of the f_2 resonance with the high mass tail of the ρ resonance. For higher masses, $m_{\pi^+\pi^-} > 1.35\,\text{GeV}$, an asymmetry with opposite sign is visible in the model, which is mainly due to the interference of the f_2 resonance with the non-resonant $\pi^+\pi^-$ production with $C = +1$ pomeron exchange. Another but smaller positive asymmetry is visible just above the $\pi^+\pi^-$ production threshold which is mainly due to the interference of $C = +1$ and $C = -1$ exchange diagrams of non-resonant $\pi^+\pi^-$ production.

We are particularly interested in the asymmetry contribution from the odderon. In figure 7(b) the total charge asymmetry is shown as function of t in the f_2 mass region $1.1\,\text{GeV} \leq m_{\pi^+\pi^-} \leq 1.35\,\text{GeV}$. A small negative asymmetry, almost constant in t, is generated by the Primakoff contribution. In contrast, a strong increase of the absolute value of the negative charge asymmetry approximately linear in $|t|$ is predicted by odderon
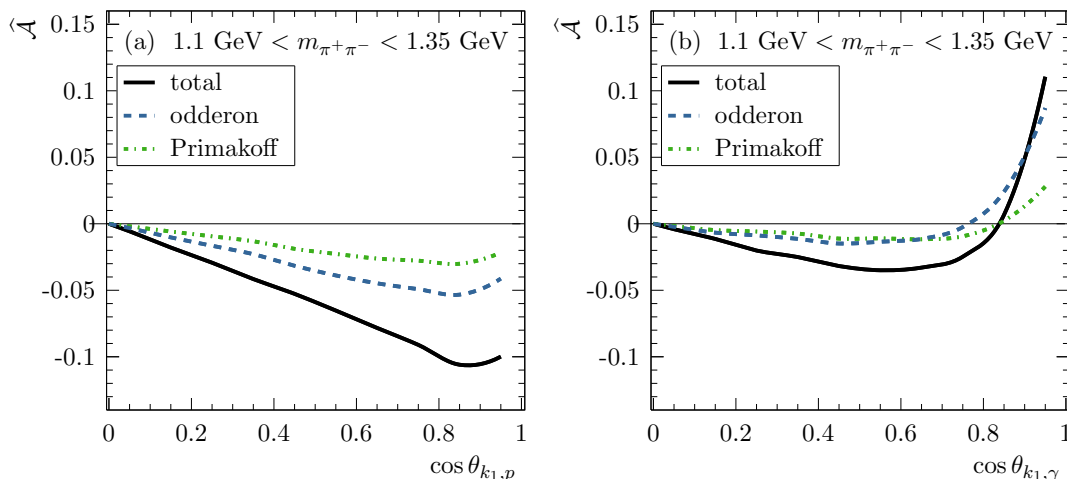
Figure 8. Charge asymmetry $\widehat{\mathcal{A}}$ (3.3) as function of the cosine of the polar angle of π^+ in the (a) proton-Jackson and (b) photon-Jackson system (see appendix A). The asymmetries are given for fixed $W_{\gamma p} = 30\,\mathrm{GeV}$ and integrated over the range $-1\,\mathrm{GeV}^2 \leq t \leq 0$ and $1.1\,\mathrm{GeV} < m_{\pi^+\pi^-} < 1.35\,\mathrm{GeV}$. The individual contributions to the asymmetries from photon (Primakoff) and odderon exchange are shown by the green dashed-dotted and blue dashed lines, respectively.

exchange with the chosen model parameters. As most events are located at low $|t|$, the experimental sensitivity to the odderon exchange diagram can be significantly enhanced by requiring a minimum $|t|$-cut, or better by measuring the approximately linear increase of the absolute value of the charge asymmetry as function of $|t|$.

Finally we compare the charge asymmetry in different systems. Figure 8(a) shows the charge asymmetry as function of $\cos\theta_{k_1,p}$ in the proton-Jackson system. The contributions from odderon and photon exchange diagrams are also shown. A strong increase of the absolute value of the asymmetry towards the forward/backward direction occurs.

Figure 8(b) shows the charge asymmetry as function of $\cos\theta_{k_1,\gamma}$ in the photon-Jackson system, in which the polar angle $\theta_{k_1,\gamma}$ is defined with respect to the incoming photon; see appendix A. For the photon-Jackson system it is interesting to note that (1) in the central region, $\cos\theta_{k_1,\gamma} \lesssim 0.6$, the asymmetry contributions due to Primakoff and odderon exchange are of similar size and (2) that the asymmetry changes sign in the polar region, $\cos\theta_{k_1,\gamma} \gtrsim 0.6$. At large $\cos\theta_{k_1,\gamma}$ the large positive asymmetry is dominated by the contribution from odderon exchange. Therefore, the photon-Jackson system offers the opportunity to study interference effects due to Primakoff and odderon exchange diagrams separately by analysing different $\cos\theta_{k_1,\gamma}$ regions. Note that due to the sign change the total asymmetry is strongly reduced (after integration over $\cos\theta_{k_1,\gamma}$) in the photon-Jackson system and that a possible odderon signal can be experimentally overlooked if only total asymmetries are studied. In the same context it should be remarked that limited detector acceptances in experimental searches might affect the measurement of angular distributions and thus the sensitivity to charge asymmetries.

The full asymmetry information of the $\pi^+\pi^-$ system can be exploited by investigating the asymmetry for all solid angles. For this study we define the angle α, which describes
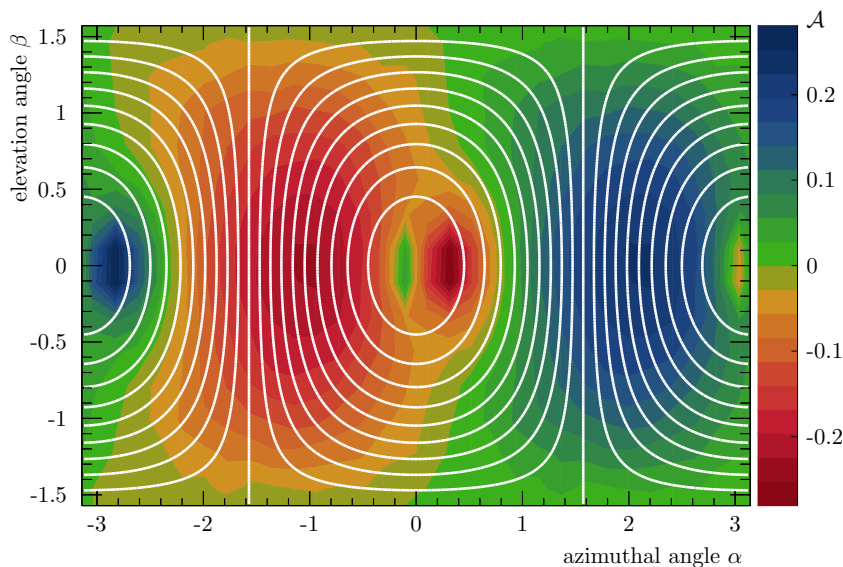
Figure 9. Charge asymmetry $\mathcal{A}$ (3.6) as function of the azimuthal angle α and the elevation angle β defined in the proton-Jackson system. The asymmetries are given for fixed $W_{\gamma p} = 30\,\mathrm{GeV}$ and integrated over the range $-1\,\mathrm{GeV}^2 \leq t \leq 0$ and $1.1\,\mathrm{GeV} < m_{\pi^+\pi^-} < 1.35\,\mathrm{GeV}$. $\alpha = 0$ corresponds to the incoming proton direction. Lines of constant polar angle $\theta_{k_1,p}$ are shown in white.

in the reaction plane the azimuthal angle of the π^+ with respect to the incoming proton beam direction, and the elevation angle β; see figure 11 and (A.20) in appendix A.

In figure 9 the charge asymmetry

$$\mathcal{A}(\alpha, \beta) = \frac{\frac{d\sigma}{d\Omega}(\alpha, \beta) - \frac{d\sigma}{d\Omega}(\alpha + \pi, -\beta)}{\frac{d\sigma}{d\Omega}(\alpha, \beta) + \frac{d\sigma}{d\Omega}(\alpha + \pi, -\beta)} \tag{3.6}$$

of the $\pi^+\pi^-$ final state is shown as function of α and β in the f_2 mass region. By construction, see (3.6), the relation $\mathcal{A}(\alpha, \beta) = -\mathcal{A}(\alpha + \pi, -\beta)$ holds. From P-invariance follows $\mathcal{A}(\alpha, \beta) = \mathcal{A}(\alpha, -\beta)$. The asymmetry distribution exhibits two dipoles: one at $\alpha \approx 0$ $(-\pi)$ related to the incoming proton direction and a second one at $\alpha \approx -\pi/2$ $(+\pi/2)$ which is broader in both α and β. For illustration, lines of constant polar angle $\theta_{k_1,p}$ are shown, along which the asymmetry was integrated to calculate the differential asymmetries for figure 8(a). The presence of complex structures in the asymmetry distribution, which are generally integrated out in one-dimensional projections, suggests to exploit the full two-dimensional information for asymmetry measurements in order to increase sensitivity and to separate the different asymmetry sources.

4 Conclusions

In this article we have presented a study of exclusive photoproduction of $\pi^+\pi^-$ pairs on protons, $\gamma p \rightarrow \pi^+\pi^- p$, in the framework of a comprehensive model for soft high-energy reactions. We have considered $\pi^+\pi^-$ production via the ρ, ω, ρ' and f_2 resonances as well as production of non-resonant $\pi^+\pi^-$ pairs. Taking into account photon, pomeron, odderon

and reggeon exchanges we have obtained analytic expressions for all contributing diagrams. We have calculated the total and various differential cross sections, angular distributions and asymmetries for a set of default parameters of the model. We emphasise that in the present paper no attempt has been made to fit data. The purpose of our paper is to provide all necessary theoretical tools for such a comparison with data.

Our methods can easily be extended to exclusive electroproduction

$$e + p \longrightarrow e + \pi^+ + \pi^- + p \tag{4.1}$$

at low to moderate values of Q^2. Another extension is to central production of $\pi^+\pi^-$ pairs in peripheral pp collisions

$$p + p \longrightarrow p + \pi^+ + \pi^- + p\,. \tag{4.2}$$

This reaction will be discussed in a forthcoming paper [56]. Central production of scalar and pseudoscalar mesons with techniques similar to the ones presented here has been discussed in [63].

In summary, we have presented a study of the reaction $\gamma p \to \pi^+\pi^- p$ in an explicit model for soft high-energy scattering that includes the exchanges of pomeron, odderon, photon, and reggeons. In particular, the model incorporates a gauge-invariant version of the Drell-Söding mechanism which is responsible for the skewing of the ρ meson shape. We have paid particular attention to the effects of the elusive odderon in the photoproduction of pion pairs. The odderon is expected to contribute to f_2 meson photoproduction as first suggested in [32, 33], and to asymmetries in the angular distribution of the $\pi^+\pi^-$ pairs as suggested in [38–44]. Our results indicate that the corresponding observables appear indeed very promising for an odderon search. More generally, we hope that our results can be used as guidance for the experimental study of interesting effects in the photoproduction of pion pairs.

Acknowledgments

A   Kinematics

Here we discuss kinematic relations for the reaction

$$\gamma^{(*)}(q, \epsilon) + p(p, \mathfrak{s}) \longrightarrow \pi^+(k_1) + \pi^-(k_2) + p'(p', \mathfrak{s}') \tag{A.1}$$

where we consider a real or virtual photon, γ or γ^*, with polarisation vector ϵ. In the final state p' stands for a proton or a diffractively excited proton, for instance the resonance $N(1520)$. The spin indices of p and p' are denoted by $\mathfrak{s}$ and $\mathfrak{s}'$, respectively. We set

$$k = k_1 + k_2\,,$$

$$s \equiv W_{\gamma p}^2 = (p + q)^2 = (p' + k)^2 \,,$$
$$t = (p' - p)^2 = (q - k)^2 \,,$$
$$m_{\pi^+\pi^-}^2 = k^2 \,, \tag{A.2}$$

and we have, in general,

$$q^2 \leq 0 \,, \qquad p'^2 \geq m_p^2 \,. \tag{A.3}$$

For the elastic photoproduction reaction (1.1) we have, of course,

$$q^2 = 0 \,, \qquad p'^2 = m_p^2 \,. \tag{A.4}$$

We denote the space-part of the four-vector p by $\mathbf{p}$, etc.

From the five momentum vectors of the particles in the reaction (A.1) we can form 15 scalar products and one parity-odd (P-odd) invariant I_P. As the P-odd invariant we can choose

$$I_P = \epsilon_{\mu\nu\rho\sigma} \, p^\mu \, q^\nu \, (k_1 - k_2)^\rho \, (k_1 + k_2)^\sigma \tag{A.5}$$

where we use the convention $\epsilon_{0123} = +1$ for the totally antisymmetric symbol $\epsilon_{\mu\nu\rho\sigma}$. This parity-odd variable cannot enter the cross section calculation for unpolarised particles since we consider a process where only the P-conserving strong and electromagnetic interactions contribute.

Not all 15 scalar products are independent. We have energy-momentum conservation

$$q + p = k_1 + k_2 + p' \tag{A.6}$$

and the mass-shell conditions

$$p^2 = m_p^2 \,, \qquad k_1^2 = k_2^2 = m_\pi^2 \,. \tag{A.7}$$

We take as independent variables

$$p'^2 \,, \quad q^2 \,, \quad s \,, \quad t \,, \quad k^2 = m_{\pi^+\pi^-}^2 \,, \quad p \cdot (k_1 - k_2) \,, \quad q \cdot (k_1 - k_2) \,. \tag{A.8}$$

All scalar products can be expressed in terms of the variables in (A.8). We get

$$p \cdot p' = \frac{1}{2} \left(p'^2 + m_p^2 - t \right) ,$$
$$p \cdot q = \frac{1}{2} \left(s - m_p^2 - q^2 \right) ,$$
$$p \cdot k_1 = \frac{1}{4} \left(s - p'^2 - q^2 + t \right) + \frac{1}{2} \, p \cdot (k_1 - k_2) \,,$$
$$p \cdot k_2 = \frac{1}{4} \left(s - p'^2 - q^2 + t \right) - \frac{1}{2} \, p \cdot (k_1 - k_2) \,,$$
$$p' \cdot q = \frac{1}{2} \left(s - m_p^2 - k^2 + t \right) ,$$
$$p' \cdot k_1 = \frac{1}{4} \left(s - p'^2 - k^2 \right) + \frac{1}{2} \, p \cdot (k_1 - k_2) + \frac{1}{2} \, q \cdot (k_1 - k_2) \,,$$
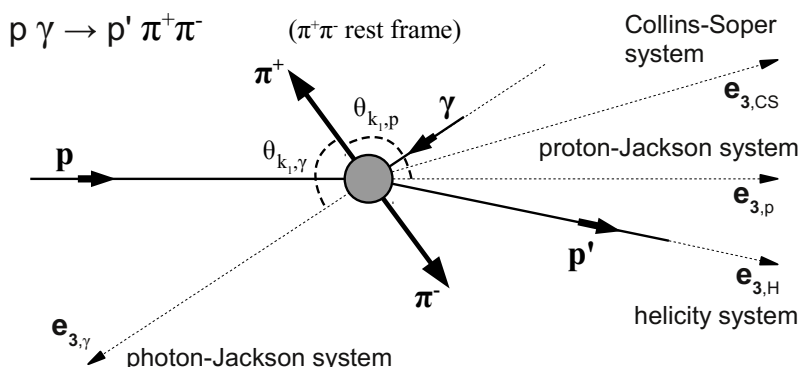
Figure 10. The reaction plane in the $\pi^+\pi^-$ rest frame and the $\mathbf{e_3}$-axes of the proton-Jackson, photon-Jackson, Collins-Soper and the helicity systems.

$$
\begin{aligned}
p' \cdot k_2 &= \frac{1}{4}\left(s - p'^2 - k^2\right) - \frac{1}{2}\, p \cdot (k_1 - k_2) - \frac{1}{2}\, q \cdot (k_1 - k_2)\,, \\
q \cdot k_1 &= \frac{1}{4}\left(q^2 + k^2 - t\right) + \frac{1}{2}\, q \cdot (k_1 - k_2)\,, \\
q \cdot k_2 &= \frac{1}{4}\left(q^2 + k^2 - t\right) - \frac{1}{2}\, q \cdot (k_1 - k_2)\,, \\
k_1 \cdot k_2 &= \frac{1}{2}\, k^2 - m_\pi^2\,.
\end{aligned}
\tag{A.9}
$$

For the photoproduction reaction (1.1) we have to insert the relations (A.4) in (A.9). Now we assume in (1.1) unpolarised photon and proton in the initial state and no observation of the polarisation of the proton in the final state. Then a complete set of kinematic variables for the reaction is given by (see (A.8))

$$
s\,,\quad t\,,\quad k^2\,,\quad p \cdot (k_1 - k_2)\,,\quad q \cdot (k_1 - k_2)\,,
\tag{A.10}
$$

and the sign of I_P. Equivalently we can choose

$$
s\,,\quad t\,,\quad k^2\,,\quad \theta\,,\quad \phi\,,
\tag{A.11}
$$

where θ, ϕ are the polar and azimuthal angles of $\mathbf{k_1}$ in the $\pi^+\pi^-$ rest system. We also note that $t \le t_{\min} < 0$ with

$$
\begin{aligned}
-t_{\min} &= 4m_p^2(k^2)^2 \left[2(s - m_p^2)^2 + 2(s - m_p^2)w(s, m_p^2, k^2) - 2(s + m_p^2)k^2\right]^{-1} \\
&= \mathcal{O}(m_p^2(k^2)^2/s^2)
\end{aligned}
\tag{A.12}
$$

where

$$
w(x, y, z) = (x^2 + y^2 + z^2 - 2xy - 2xz - 2yz)^{\frac{1}{2}}\,.
\tag{A.13}
$$

We are interested in the angular distribution of the π^+ in the centre-of-mass system of the $\pi^+\pi^-$ pair. There we have

$$
\mathbf{k} = 0\,,\qquad \mathbf{p} + \mathbf{q} = \mathbf{p}'\,.
\tag{A.14}
$$

Various reference systems are commonly used; see figure 10 for illustration. We list here the proton and photon-Jackson systems, see [64, 65], which are used in section 3 to illustrate cross sections and asymmetries. In addition we also mention the Collins-Soper [66] and the helicity system [67].

For the proton-Jackson system we set (cf. p. 125 of [67])

$$\mathbf{e_{1,}}_p = \frac{-\mathbf{p}' + \hat{\mathbf{p}}(\hat{\mathbf{p}} \cdot \mathbf{p}')}{|\hat{\mathbf{p}} \times \mathbf{p}'|},$$

$$\mathbf{e_{2,}}_p = -\frac{\hat{\mathbf{p}} \times \mathbf{p}'}{|\hat{\mathbf{p}} \times \mathbf{p}'|},$$

$$\mathbf{e_{3,}}_p = \hat{\mathbf{p}},\tag{A.15}$$

with $\hat{\mathbf{p}} = \mathbf{p}/|\mathbf{p}|$, $\hat{\mathbf{q}} = \mathbf{q}/|\mathbf{q}|$ and $\mathbf{p}$, $\mathbf{q}$ the three-momenta of the initial proton and the $\gamma^{(*)}$ in the $\pi^+\pi^-$ rest system. The corresponding polar and azimuthal angles of the π^+ are denoted by $\theta_{k_1,p}$ and $\phi_{k_1,p}$, respectively, and we have $\cos\theta_{k_1,p} = \hat{\mathbf{k}}_1 \cdot \hat{\mathbf{p}}$.

For the photon-Jackson system we set (cf. p. 125 of [67])

$$\mathbf{e_{1,}}_\gamma = \frac{-\mathbf{p}' + \hat{\mathbf{q}}(\hat{\mathbf{q}} \cdot \mathbf{p}')}{|\hat{\mathbf{q}} \times \mathbf{p}'|},$$

$$\mathbf{e_{2,}}_\gamma = -\frac{\hat{\mathbf{q}} \times \mathbf{p}'}{|\hat{\mathbf{q}} \times \mathbf{p}'|},$$

$$\mathbf{e_{3,}}_\gamma = \hat{\mathbf{q}}.\tag{A.16}$$

The polar and azimuthal angles of the π^+ in the photon-Jackson system are denoted by $\theta_{k_1,\gamma}$ and $\phi_{k_1,\gamma}$, respectively, and we have $\cos\theta_{k_1,\gamma} = \hat{\mathbf{k}}_1 \cdot \hat{\mathbf{q}}$.

We mention two more systems of reference, the Collins-Soper and the helicity systems. The unit vectors of the CS system are chosen as

$$\mathbf{e_{1,}}_{\mathrm{CS}} = \frac{\hat{\mathbf{p}} + \hat{\mathbf{q}}}{|\hat{\mathbf{p}} + \hat{\mathbf{q}}|},$$

$$\mathbf{e_{2,}}_{\mathrm{CS}} = \frac{\hat{\mathbf{p}} \times \hat{\mathbf{q}}}{|\hat{\mathbf{p}} \times \hat{\mathbf{q}}|},$$

$$\mathbf{e_{3,}}_{\mathrm{CS}} = \frac{\hat{\mathbf{p}} - \hat{\mathbf{q}}}{|\hat{\mathbf{p}} - \hat{\mathbf{q}}|},\tag{A.17}$$

and the unit vectors of the helicity system are chosen as

$$\mathbf{e_{1,}}_{\mathrm{H}} = \frac{\mathbf{q} - \hat{\mathbf{p}}'(\hat{\mathbf{p}}' \cdot \mathbf{q})}{|\mathbf{q} \times \hat{\mathbf{p}}'|},$$

$$\mathbf{e_{2,}}_{\mathrm{H}} = \frac{\hat{\mathbf{p}}' \times \mathbf{q}}{|\hat{\mathbf{p}}' \times \mathbf{q}|},$$

$$\mathbf{e_{3,}}_{\mathrm{H}} = \hat{\mathbf{p}}',\tag{A.18}$$

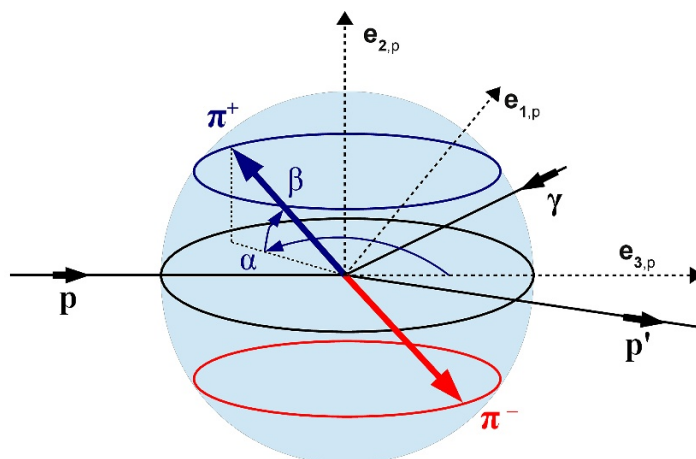with $\hat{\mathbf{p}}' = \mathbf{p}'/|\mathbf{p}'|$.

Figure 11. Definition of the angles α and β in the $\pi^+\pi^-$ rest frame. As reference the proton-Jackson system is chosen. We have $0 \le \alpha < 2\pi$ and $-\pi/2 \le \beta \le \pi/2$.

All systems discussed above have the $\mathbf{e_1}$ and $\mathbf{e_3}$ unit vectors in the reaction plane given by the incoming and outgoing protons. With the above definitions we obtain the relation

$$\mathbf{e}_{2,p} = -\mathbf{e}_{2,\gamma} = -\mathbf{e}_{2,\mathrm{CS}} = -\mathbf{e}_{2,\mathrm{H}}. \tag{A.19}$$

The directions of the vectors $\mathbf{e_3}$ in the different systems are shown in figure 10. They differ only by their orientation with respect to rotations around the $\mathbf{e_2}$ axis.

This property, and the fact that P-invariance with respect to reflection at the reaction plane holds, motivates to define two new angles α and β. These angles describe the direction of the π^+ in the $\pi^+\pi^-$ rest frame and are defined as

$$\sin\beta = \hat{\mathbf{k}}_\mathbf{1} \cdot \mathbf{e}_{2,p} = -\frac{\hat{\mathbf{k}}_\mathbf{1} \cdot (\hat{\mathbf{p}} \times \mathbf{p}')}{|\hat{\mathbf{p}} \times \mathbf{p}'|},$$

$$\cos\beta \cos\alpha = \hat{\mathbf{k}}_\mathbf{1} \cdot \mathbf{e}_{3,p} = \hat{\mathbf{k}}_\mathbf{1} \cdot \hat{\mathbf{p}},$$

$$\cos\beta \sin\alpha = \hat{\mathbf{k}}_\mathbf{1} \cdot \mathbf{e}_{1,p} = \frac{-\hat{\mathbf{k}}_\mathbf{1} \cdot \mathbf{p}' + (\hat{\mathbf{k}}_\mathbf{1} \cdot \hat{\mathbf{p}})(\hat{\mathbf{p}} \cdot \mathbf{p}')}{|\hat{\mathbf{p}} \times \mathbf{p}'|}, \tag{A.20}$$

where $\alpha = 0$ is aligned to the incoming proton direction. Note that α and β can also be interpreted as the spherical coordinates of the π^+ in the $\pi^+\pi^-$ rest frame, with $\mathbf{e}_{2,p}$ having the rôle of the z- and $\mathbf{e}_{3,p}$ the rôle of the x-axis.

Transformation from one system i to another system j from (A.15) to (A.18) can then be represented by rotations:

$$\alpha_i \rightarrow \alpha_j + \Delta\alpha_{ij}. \tag{A.21}$$

Reflections with respect to the reaction plane are described by a transformation of the elevation angle $\beta \rightarrow -\beta$ and P-invariance requires

$$\frac{d\sigma}{d\Omega}(\alpha, \beta) = \frac{d\sigma}{d\Omega}(\alpha, -\beta). \tag{A.22}$$

The following relations between the angles α, β and $\theta_{k_1,p}$, $\phi_{k_1,p}$ in the proton-Jackson system hold:

$$\tan\alpha \;=\; \tan\theta_{k_1,p}\,\cos\phi_{k_1,p}\,, \tag{A.23}$$

$$\sin\beta \;=\; \sin\theta_{k_1,p}\,\sin\phi_{k_1,p}\,. \tag{A.24}$$
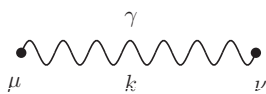
B Propagators and vertices

In this appendix we collect the propagators and vertices needed for the evaluation of the diagrams of figure 1. Here the propagators and vertices involving the pomeron, the odderon and the reggeons are to be understood as effective propagators and vertices. Most of the relations listed in the following are taken over from [28]. We reproduce them here in order to make the present paper self-contained.

The numerical values of coupling constants and other parameters quoted in the following are to be considered as default values. Adjustments of these parameters should come from detailed comparisons with experiment.

All our vertices respect the standard crossing and charge-conjugation (C) relations of quantum field theory.

Propagators:

- photon γ:
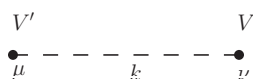
$$i\Delta_{\mu\nu}^{(\gamma)}(k) = \frac{-ig_{\mu\nu}}{k^2 + i\epsilon}\,. \tag{B.1}$$

- pions π^0, $\pi^\pm$:

$$i\Delta^{(\pi)}(k) = \frac{i}{k^2 - m_\pi^2 + i\epsilon}\,. \tag{B.2}$$

- vector-mesons $V = \rho^0, \omega$: Since we include in our calculations ρ^0–ω interference effects we rely here on the analysis of the γ–ρ–ω propagator matrix as given in [68]. But here we are only interested in the ρ–ω, the strong-interaction, part of the 3×3 propagator matrix studied there. We get the following from appendix B of [68], setting $e = 0$ in the relations there, for $V', V \in \{\rho, \omega\}$:

$$i\Delta_{\mu\nu}^{(V',V)}(k) = i\left(-g_{\mu\nu} + \frac{k_\mu k_\nu}{k^2 + i\epsilon}\right)\Delta_T^{(V',V)}(k^2) - i\frac{k_\mu k_\nu}{k^2 + i\epsilon}\Delta_L^{(V',V)}(k^2). \tag{B.3}$$

Here and in the following ρ is understood as ρ^0. The longitudinal parts $\Delta_L^{(V',V)}(k^2)$ never enter in our calculations and, thus, need not be discussed further. For the transverse parts we use matrix notation. With $k^2 = s$ we set

$$\underline{\Delta}_T(s) = \begin{pmatrix} \Delta_T^{(\rho,\rho)}(s) & \Delta_T^{(\rho,\omega)}(s) \\ \Delta_T^{(\omega,\rho)}(s) & \Delta_T^{(\omega,\omega)}(s) \end{pmatrix}. \tag{B.4}$$

We have from [68] where all these relations are derived and discussed at length:

$$\Delta_T^{(\omega,\rho)}(s) = \Delta_T^{(\rho,\omega)}(s), \tag{B.5}$$

$$(\underline{\Delta}_T(s))^{-1} = \begin{pmatrix} -m_\rho^2 + s + B_{\rho\rho}(s) & sb_{\rho\omega} + B_{\rho\omega}(s) \\ sb_{\rho\omega} + B_{\rho\omega}(s) & -m_\omega^2 + s + B_{\omega\omega}(s) \end{pmatrix}, \tag{B.6}$$

$$\begin{aligned} & B_{V'V}(s=0) = 0, \\ & \mathrm{Re}\, B_{\rho\rho}(m_\rho^2) = \mathrm{Re}\, B_{\rho\omega}(m_\rho^2) = 0, \\ & \mathrm{Re}\, B_{\omega\omega}(m_\omega^2) = 0, \end{aligned} \tag{B.7}$$

$$\underline{\Delta}_T(s=0) = \begin{pmatrix} -\frac{1}{m_\rho^2} & 0 \\ 0 & -\frac{1}{m_\omega^2} \end{pmatrix}, \tag{B.8}$$

$$\begin{aligned} B_{\rho\rho}(s) = {}& g_{\rho\pi\pi}^2 s\left[R(s, m_\pi^2) - R(m_\rho^2, m_\pi^2) + \frac{1}{2}\left(R(s, m_K^2) - R(m_\rho^2, m_K^2)\right)\right] \\ & + ig_{\rho\pi\pi}^2\left[I(s, m_\pi^2) + \frac{1}{2}I(s, m_K^2)\right], \end{aligned} \tag{B.9}$$

$$I(s, m^2) = \frac{1}{192\pi}s\left(1 - \frac{4m^2}{s}\right)^{3/2}\theta(s - 4m^2), \tag{B.10}$$

$$R(s, m^2) = \frac{s}{192\pi^2}\,\mathrm{V.P.}\int_{4m^2}^{\infty}\frac{ds'}{s'(s'-s)}\left(1 - \frac{4m^2}{s'}\right)^{\frac{3}{2}}. \tag{B.11}$$

Here V. P. means the principal value prescription. Explicitly we get the following. For $s > 4m^2$

$$R(s, m^2) = \frac{1}{96\pi^2}\left[\frac{1}{3} + \xi^2 + \frac{1}{2}\xi^3\log\left(\frac{1-\xi}{1+\xi}\right)\right] \quad\text{with}\quad \xi = \left(1 - \frac{4m^2}{s}\right)^{1/2}, \tag{B.12}$$

for $0 < s < 4m^2$

$$R(s, m^2) = \frac{1}{96\pi^2}\left[\frac{1}{3} - \xi^2 + \xi^3\arctan\left(\frac{1}{\xi}\right)\right] \quad\text{with}\quad \xi = \left(\frac{4m^2}{s} - 1\right)^{1/2}, \tag{B.13}$$

and for $s < 0$

$$R(s, m^2) = \frac{1}{96\pi^2}\left[\frac{1}{3} + \xi^2 + \frac{1}{2}\xi^3\log\left(\frac{\xi-1}{\xi+1}\right)\right] \quad\text{with}\quad \xi = \left(1 - \frac{4m^2}{s}\right)^{1/2}. \tag{B.14}$$

Furthermore, we have from [68]

$$B_{\omega\omega}(s) = g_{\omega KK}^2 s \left[R(s, m_K^2) - R(m_\omega^2, m_K^2) \right] + i\frac{s}{m_\omega}\Gamma_\omega \,, \qquad g_{\omega KK} = \frac{1}{2}g_{\rho\pi\pi}\,, \quad \text{(B.15)}$$

$$B_{\rho\omega}(s) = g_{\rho\pi\pi}g_{\omega\pi\pi} \left[s\left(R(s, m_\pi^2) - R(m_\rho^2, m_\pi^2) \right) + iI(s, m_\pi^2) \right]. \quad \text{(B.16)}$$

In [68] fits to the pion electromagnetic, weak, and $\pi\gamma$ transition form factors were made. From the fit III in table 4 of [68] the following values for the parameters of $\underline{\Delta}_T(s)$ (B.4) were determined:

$$
\begin{aligned}
m_\rho &= 773.7 \pm 0.4 \,\text{MeV}\,, \\
m_\omega &= 782.43 \pm 0.05 \,\text{MeV}\,, \\
\Gamma_\omega &= 8.49 \pm 0.08 \,\text{MeV}\,, \quad \text{(input from [69])} \\
g_{\rho\pi\pi} &= 11.51 \pm 0.07\,, \\
g_{\omega\pi\pi} &= -0.35 \pm 0.10\,, \\
b_{\rho\omega} &= (3.5 \pm 0.5) \times 10^{-3}\,.
\end{aligned}
\qquad \text{(B.17)}
$$

For comparison we quote the ρ and ω masses as listed in [69]:

$$
\begin{aligned}
m_\rho &= 775.26 \pm 0.25 \,\text{MeV}\,, \\
m_\omega &= 782.65 \pm 0.12 \,\text{MeV}\,.
\end{aligned}
\qquad \text{(B.18)}
$$

These values are quite consistent with the corresponding ones from (B.17). We recall that we are only quoting default values for our calculations here and for this purpose it makes no difference if we take those from (B.17) or from (B.18). The definitions of the coupling constants $g_{\rho\pi\pi}$ and $g_{\omega\pi\pi}$ through the corresponding vertices are given in (B.55) below.

The ρ–ω propagator matrix as defined above should be a good model for $|s| \lesssim 15 \,\text{GeV}^2$; see section 4 of [28].

- vector-meson ρ':
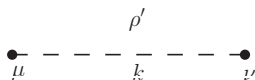
$$i\Delta_{\mu\nu}^{(\rho',\rho')}(k) = i\left(-g_{\mu\nu} + \frac{k_\mu k_\nu}{k^2 + i\epsilon} \right)\Delta_T^{(\rho',\rho')}(k^2) - i\frac{k_\mu k_\nu}{k^2 + i\epsilon}\Delta_L^{(\rho',\rho')}(k^2)\,. \quad \text{(B.19)}$$

Again, $\Delta_L^{(\rho',\rho')}(k^2)$ need not be discussed. For $\Delta_T^{(\rho',\rho')}(k^2)$ we make a simple ansatz as suggested in [70]

$$\Delta_T^{(\rho',\rho')}(s) = \frac{1}{s - m_{\rho'}^2 + i\sqrt{s}\,\Gamma_{\rho'}(s)}\,, \quad \text{(B.20)}$$

$$\Gamma_{\rho'}(s) = \Gamma_{\rho'}\left(\frac{s - 4m_\pi^2}{m_{\rho'}^2 - 4m_\pi^2} \right)^{3/2} \frac{m_{\rho'}^2}{s}\,\theta(s - 4m_\pi^2)\,. \quad \text{(B.21)}$$

The values for $m_{\rho'}$ and $\Gamma_{\rho'}$ listed in [69] are

$$m_{\rho'} = 1465 \pm 25\,\text{MeV}\,,$$
$$\Gamma_{\rho'} = 400 \pm 60\,\text{MeV}\,. \tag{B.22}$$

We note that in [71] — contrary to what is written there — a different form for the ρ' propagator is used, *not* the one from [70] which we reproduce here in (B.20), (B.21). The Breit-Wigner ansatz made in eqs. (4), (5) of [71] corresponds to replacing in (B.20) $\sqrt{s}\,\Gamma_{\rho'}(s)$ by $m_{\rho'}\Gamma_{\rho'}(s)$. We shall not use such a form for the ρ' propagator.

- tensor meson $f_2 \equiv f_2(1270)$ (see (3.6)–(3.9)) and section 5 of [28]):

$$i\Delta^{(f_2)}_{\mu\nu,\kappa\lambda}(k) = i\left\{\frac{1}{2}\left(-g_{\mu\kappa} + \frac{k_\mu k_\kappa}{k^2 + i\epsilon}\right)\left(-g_{\nu\lambda} + \frac{k_\nu k_\lambda}{k^2 + i\epsilon}\right)\right.$$
$$+ \frac{1}{2}\left(-g_{\mu\lambda} + \frac{k_\mu k_\lambda}{k^2 + i\epsilon}\right)\left(-g_{\nu\kappa} + \frac{k_\nu k_\kappa}{k^2 + i\epsilon}\right) \tag{B.23}$$
$$\left. - \frac{1}{3}\left(-g_{\mu\nu} + \frac{k_\mu k_\nu}{k^2 + i\epsilon}\right)\left(-g_{\kappa\lambda} + \frac{k_\kappa k_\lambda}{k^2 + i\epsilon}\right)\right\}\Delta^{(2)}(k^2)\,.$$

Here we suppose $0 < k^2 < 10\,\text{GeV}^2$. The invariant function $\Delta^{(2)}(k^2)$ is given as follows, setting $k^2 = s$,

$$\left[\Delta^{(2)}(s)\right]^{-1} = -m_{f_2}^2 + s + s\left[R_{f_2}(s) - R_{f_2}(m_{f_2}^2)\right] + i\,\text{Im}\,B_{f_2}(s)\,, \tag{B.24}$$

with

$$\text{Im}\,B_{f_2}(s) = \frac{\Gamma_{f_2}}{\Gamma(f_2 \to \pi\pi)}\frac{1}{320\pi}\left|\frac{g_{f_2\pi\pi}F^{(f_2\pi\pi)}(s)}{M_0}\right|^2 s^2\left(1 - \frac{4m_\pi^2}{s}\right)^{\frac{5}{2}}\theta(s - 4m_\pi^2)\,, \tag{B.25}$$

$$R_{f_2}(s) = \frac{s}{\pi}\,\text{V.P.}\int_{4m_\pi^2}^{\infty}ds'\,\frac{\text{Im}\,B_{f_2}(s')}{s'^2(s' - s)}\,, \tag{B.26}$$

where V. P. means the principal value prescription and $M_0 = 1\,\text{GeV}$; see (5.19)–(5.22) of [28]. The coupling constant $g_{f_2\pi\pi}$ and the form factor $F^{(f_2\pi\pi)}(s)$ are defined in (3.37) and (5.4) of [28]; see (B.58)–(B.60) below.

The following relations hold:

$$\Delta^{(f_2)}_{\mu\nu,\kappa\lambda}(k) = \Delta^{(f_2)}_{\nu\mu,\kappa\lambda}(k) = \Delta^{(f_2)}_{\mu\nu,\lambda\kappa}(k) = \Delta^{(f_2)}_{\kappa\lambda,\mu\nu}(k)\,, \tag{B.27}$$
$$g^{\mu\nu}\Delta^{(f_2)}_{\mu\nu,\kappa\lambda}(k) = 0\,, \tag{B.28}$$
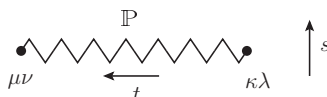$$g^{\kappa\lambda}\Delta^{(f_2)}_{\mu\nu,\kappa\lambda}(k) = 0\,.$$

From [69] we get the mass and width of the f_2 meson as

$$m_{f_2} = 1275.1 \pm 1.2\,\text{MeV}\,, \qquad \Gamma_{f_2} = 185.1\,^{+2.9}_{-2.4}\,\text{MeV}\,, \tag{B.29}$$

and the $f_2 \to \pi\pi$ branching fraction as

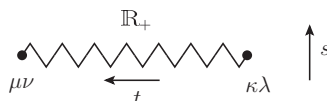$$\frac{\Gamma(f_2 \to \pi\pi)}{\Gamma_{f_2}} = (84.8^{+2.4}_{-1.2})\,. \tag{B.30}$$

- pomeron $\mathbb{P}$ (see (3.10), (3.11) and section 6.1 of [28]):

$$i\Delta^{(\mathbb{P})}_{\mu\nu,\kappa\lambda}(s,t) = \frac{1}{4s}\left(g_{\mu\kappa}g_{\nu\lambda} + g_{\mu\lambda}g_{\nu\kappa} - \frac{1}{2}g_{\mu\nu}g_{\kappa\lambda}\right)(-is\alpha'_{\mathbb{P}})^{\alpha_{\mathbb{P}}(t)-1}\,, \tag{B.31}$$

$$\alpha_{\mathbb{P}}(t) = 1 + \epsilon_{\mathbb{P}} + \alpha'_{\mathbb{P}}t\,,$$
$$\epsilon_{\mathbb{P}} = 0.0808\,, \tag{B.32}$$
$$\alpha'_{\mathbb{P}} = 0.25\,\text{GeV}^{-2}\,.$$

- reggeons $\mathbb{R}_+ = f_{2R}, a_{2R}$ (see (3.12), (3.13) and section 6.3 of [28]):

$$i\Delta^{(\mathbb{R}_+)}_{\mu\nu,\kappa\lambda}(s,t) = \frac{1}{4s}\left(g_{\mu\kappa}g_{\nu\lambda} + g_{\mu\lambda}g_{\nu\kappa} - \frac{1}{2}g_{\mu\nu}g_{\kappa\lambda}\right)(-is\alpha'_{\mathbb{R}_+})^{\alpha_{\mathbb{R}_+}(t)-1}\,, \tag{B.33}$$

$$\alpha_{\mathbb{R}_+}(t) = \alpha_{\mathbb{R}_+}(0) + \alpha'_{\mathbb{R}_+}t\,,$$
$$\alpha_{\mathbb{R}_+}(0) = 0.5475\,, \tag{B.34}$$
$$\alpha'_{\mathbb{R}_+} = 0.9\,\text{GeV}^{-2}\,.$$

- reggeons $\mathbb{R}_- = \omega_R, \rho_R$ (see (3.14), (3.15) and section 6.3 of [28]):
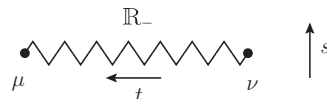
$$i\Delta^{(\mathbb{R}_-)}_{\mu\nu}(s,t) = ig_{\mu\nu}\frac{1}{M_-^2}(-is\alpha'_{\mathbb{R}_-})^{\alpha_{\mathbb{R}_-}(t)-1}\,, \tag{B.35}$$

$$\alpha_{\mathbb{R}_-}(t) = \alpha_{\mathbb{R}_-}(0) + \alpha'_{\mathbb{R}_-}t\,,$$
$$\alpha_{\mathbb{R}_-}(0) = 0.5475\,,$$
$$\alpha'_{\mathbb{R}_-} = 0.9\,\text{GeV}^{-2}\,, \tag{B.36}$$
$$M_- = 1.41\,\text{GeV}\,.$$

- odderon $\mathbb{O}$ (see (3.16), (3.17) and section 6.2 of [28]):
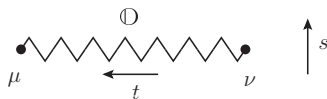
$$i\Delta_{\mu\nu}^{(\mathbb{O})}(s,t) = -ig_{\mu\nu}\frac{\eta_{\mathbb{O}}}{M_0^2}\left(-is\alpha_{\mathbb{O}}'\right)^{\alpha_{\mathbb{O}}(t)-1}, \tag{B.37}$$

$$\alpha_{\mathbb{O}}(t) = 1 + \epsilon_{\mathbb{O}} + \alpha_{\mathbb{O}}'t,$$
$$\eta_{\mathbb{O}} = \pm 1, \tag{B.38}$$
$$\alpha_{\mathbb{O}}' = 0.25\,\text{GeV}^{-2}.$$

We have set as default $\alpha_{\mathbb{O}}' = \alpha_{\mathbb{P}}'$ in (B.38).

Vertices: in this section we list the vertices which are needed for discussing the reaction (1.1). We use as in [28] the following rank-four tensor functions

$$\Gamma_{\mu\nu\kappa\lambda}^{(0)}(k_1,k_2) = [(k_1\cdot k_2)g_{\mu\nu} - k_{2\mu}k_{1\nu}]\left[k_{1\kappa}k_{2\lambda} + k_{2\kappa}k_{1\lambda} - \frac{1}{2}(k_1\cdot k_2)g_{\kappa\lambda}\right], \tag{B.39}$$

$$\Gamma_{\mu\nu\kappa\lambda}^{(2)}(k_1,k_2) = (k_1\cdot k_2)(g_{\mu\kappa}g_{\nu\lambda} + g_{\mu\lambda}g_{\nu\kappa}) + g_{\mu\nu}(k_{1\kappa}k_{2\lambda} + k_{2\kappa}k_{1\lambda})$$

$$- k_{1\nu}k_{2\lambda}g_{\mu\kappa} - k_{1\nu}k_{2\kappa}g_{\mu\lambda} - k_{2\mu}k_{1\lambda}g_{\nu\kappa} - k_{2\mu}k_{1\kappa}g_{\nu\lambda} \tag{B.40}$$

$$- [(k_1\cdot k_2)g_{\mu\nu} - k_{2\mu}k_{1\nu}]g_{\kappa\lambda}.$$

For $i = 0,2$ we have

$$\Gamma_{\mu\nu\kappa\lambda}^{(i)}(k_1,k_2) = \Gamma_{\mu\nu\lambda\kappa}^{(i)}(k_1,k_2) = \Gamma_{\nu\mu\kappa\lambda}^{(i)}(k_2,k_1) = \Gamma_{\mu\nu\kappa\lambda}^{(i)}(-k_1,-k_2), \tag{B.41}$$

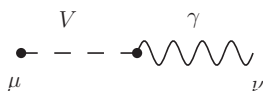$$k_1^\mu\Gamma_{\mu\nu\kappa\lambda}^{(i)}(k_1,k_2) = 0, \tag{B.42}$$

$$k_2^\nu\Gamma_{\mu\nu\kappa\lambda}^{(i)}(k_1,k_2) = 0,$$

$$\Gamma_{\mu\nu\kappa\lambda}^{(i)}(k_1,k_2)\,g^{\kappa\lambda} = 0. \tag{B.43}$$

The vertices read as follows.

- γV, where $V = \rho,\omega,\phi,\rho'$ (see (3.23)–(3.25) and section 4 of [28]):
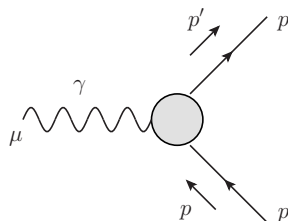

$$-ie\frac{m_V^2}{\gamma_V}g_{\mu\nu}, \tag{B.44}$$

$$e > 0, \quad \gamma_\rho > 0, \quad \gamma_\omega > 0, \quad \gamma_\phi < 0, \tag{B.45}$$

$$\frac{4\pi}{\gamma_\rho^2} = 0.496 \pm 0.023, \quad \frac{4\pi}{\gamma_\omega^2} = 0.042 \pm 0.0015, \quad \frac{4\pi}{\gamma_\phi^2} = 0.0716 \pm 0.0017. \tag{B.46}$$

A reliable determination of $\gamma_{\rho'}$ is not known to us.

- γpp (see (3.26)–(3.32) of [28]):

$$i\Gamma_\mu^{(\gamma pp)}(p',p) = -ie\left[\gamma_\mu F_1(t) + \frac{i}{2m_p}\sigma_{\mu\nu}(p'-p)^\nu F_2(t)\right], \qquad \text{(B.47)}$$

$$e > 0, \qquad t = (p'-p)^2, \qquad \text{(B.48)}$$

$$\sigma_{\mu\nu} = \frac{i}{2}\left(\gamma_\mu\gamma_\nu - \gamma_\nu\gamma_\mu\right), \qquad \text{(B.49)}$$

$$F_1(t) = \left(1 - \frac{t}{4m_p^2}\frac{\mu_p}{\mu_N}\right)\left(1 - \frac{t}{4m_p^2}\right)^{-1}G_D(t), \qquad \text{(B.50)}$$

$$F_2(t) = \left(\frac{\mu_p}{\mu_N} - 1\right)\left(1 - \frac{t}{4m_p^2}\right)^{-1}G_D(t), \qquad \text{(B.51)}$$

$$\mu_N = \frac{e}{2m_p}, \qquad\qquad \frac{\mu_p}{\mu_N} = 2.7928, \qquad \text{(B.52)}$$

$$G_D(t) = \left(1 - \frac{t}{m_D^2}\right)^{-2}, \qquad m_D^2 = 0.71\,\text{GeV}^2. \qquad \text{(B.53)}$$

The proton's Dirac and Pauli form factors and the dipole form factor are denoted by F_1, F_2, and G_D, respectively; see for instance chapter 2 in [3].

In many hadronic vertices we have, realistically, to introduce form factors. For simplicity we use for the proton for momentum transfer squared $t < 0$ in general the Dirac form factor $F_1(t)$ (B.50). For mesons we use for $t < 0$ a simple parametrisation of the pion's electromagnetic form factor

$$F_M(t) = F_\pi(t) = \frac{m_0^2}{m_0^2 - t}, \qquad m_0^2 = 0.50\,\text{GeV}^2; \qquad \text{(B.54)}$$

see (3.34) of [28]. Further form factors are introduced and discussed below.

- $V\pi^+\pi^-$, $V = \rho, \omega, \rho'$ (see [68] and section 4 of [28]):
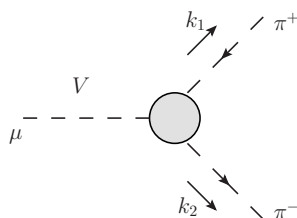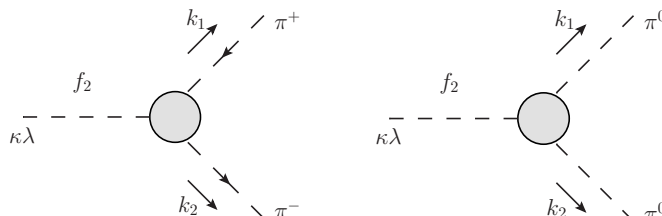

$$i\Gamma_\mu^{(V\pi\pi)}(k_1, k_2) = -\frac{1}{2}ig_{V\pi\pi}(k_1 - k_2)_\mu, \qquad \text{(B.55)}$$

$$g_{\rho\pi\pi} = 11.51 \pm 0.07 \,, \tag{B.56}$$

$$g_{\omega\pi\pi} = -0.35 \pm 0.10 \,. \tag{B.57}$$

As default values for the $\rho\pi\pi$ and $\omega\pi\pi$ coupling constants we take those from table 4 of [68]. For $g_{\rho'\pi\pi}$ we have no reliable estimate.

- $f_2\pi\pi$ (see (3.37), (3.38) and section 5.1 of [28]):

$$i\Gamma^{(f_2\pi\pi)}_{\kappa\lambda}(k_1, k_2) = -i\frac{g_{f_2\pi\pi}}{2M_0}\left[(k_1-k_2)_\kappa(k_1-k_2)_\lambda - \frac{1}{4}g_{\kappa\lambda}(k_1-k_2)^2\right]F^{(f_2\pi\pi)}(k^2)\,, \tag{B.58}$$

where $k = k_1 + k_2$ and

$$g_{f_2\pi\pi} = 9.26 \pm 0.15 \,. \tag{B.59}$$

A convenient form for the $F^{(f_2\pi\pi)}$ form factor is

$$F^{(f_2\pi\pi)}(k^2) = \exp\left(-\frac{k^2 - m_{f_2}^2}{\Lambda_{f_2}^2}\right) \tag{B.60}$$

which satisfies $F^{(f_2\pi\pi)}(m_{f_2}^2) = 1$. The parameter Λ_{f_2} is estimated to be in the range 1 to 4 GeV.

- $f_2\gamma\gamma$ (see (3.39), (3.40) and sections 5.3, 7.2 of [28]):
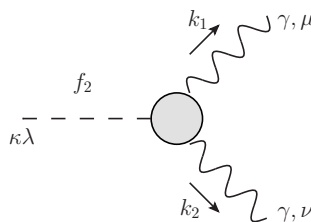
$$i\Gamma^{(f_2\gamma\gamma)}_{\mu\nu\kappa\lambda}(k_1, k_2) = iF_M(k_1^2)F_M(k_2^2)F^{(f_2\gamma\gamma)}(k^2) \tag{B.61}$$
$$\times\left[2a_{f_2\gamma\gamma}\Gamma^{(0)}_{\mu\nu\kappa\lambda}(k_1, k_2) - b_{f_2\gamma\gamma}\Gamma^{(2)}_{\mu\nu\kappa\lambda}(k_1, k_2)\right]\,.$$
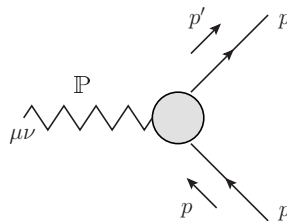
Here $k = k_1 + k_2$ and

$$a_{f_2\gamma\gamma} = \frac{e^2}{4\pi}\,1.45\,\text{GeV}^{-3}\,, \qquad b_{f_2\gamma\gamma} = \frac{e^2}{4\pi}\,2.49\,\text{GeV}^{-1}\,. \tag{B.62}$$

The form factor $F^{(f_2\gamma\gamma)}(k^2)$ is taken to be the same as for the $f_2\pi\pi$ vertex in (B.60),

$$F^{(f_2\gamma\gamma)}(k^2) = F^{(f_2\pi\pi)}(k^2)\,. \tag{B.63}$$

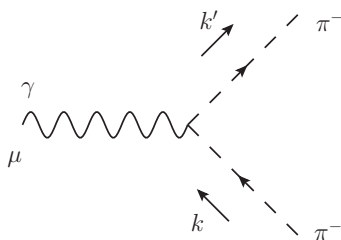- $\mathbb{P}pp$ (see (3.43), (3.44) and section 6.1 of [28]):

$$i\Gamma_{\mu\nu}^{(\mathbb{P}pp)}(p',p) = -i\,3\beta_{\mathbb{P}NN}F_1[(p'-p)^2]$$

$$\times \left\{ \frac{1}{2}\left[\gamma_\mu(p'+p)_\nu + \gamma_\nu(p'+p)_\mu\right] - \frac{1}{4}\,g_{\mu\nu}(\not{p}'+\not{p}) \right\}, \quad \text{(B.64)}$$

$$\beta_{\mathbb{P}NN} = 1.87\,\text{GeV}^{-1}. \quad \text{(B.65)}$$
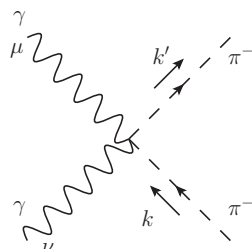
- $\gamma\pi\pi$, $\gamma\gamma\pi\pi$, $\mathbb{P}\pi\pi$, $\mathbb{P}\gamma\pi\pi$ (see (3.45), (3.46), and section 7.1 of [28]): Our starting point here is the pion Lagrangian including the $\mathbb{P}\pi\pi$ coupling term as written in (7.3) of [28]. Making a minimal substitution there in order to include the coupling to the photon leads to

$$\begin{aligned}
\mathcal{L}(x) = &\left[(\partial_\mu - ieA_\mu(x))\pi^-(x)\right](\partial^\mu + ieA^\mu(x))\,\pi^+(x)\\
&+ \frac{1}{2}\left(\partial_\mu\pi^0(x))(\partial^\mu\pi^0(x)\right) - m_\pi^2\left(\pi^-(x)\pi^+(x) + \frac{1}{2}\pi^0(x)\pi^0(x)\right)\\
&+ 2\beta_{\mathbb{P}\pi\pi}\mathbb{P}_{\kappa\lambda}(x)\left(g^{\kappa\mu}g^{\lambda\nu} - \frac{1}{4}g^{\kappa\lambda}g^{\mu\nu}\right)\\
&\times \Bigg\{\pi^-(x)(\partial_\mu + ieA_\mu(x))(\partial_\nu + ieA_\nu(x))\,\pi^+(x)\\
&\quad + \left[(\partial_\mu - ieA_\mu(x))(\partial_\nu - ieA_\nu(x))\pi^-(x)\right]\pi^+(x)\\
&\quad - \left[(\partial_\mu - ieA_\mu(x))\pi^-(x)\right]\left[(\partial_\nu + ieA_\nu(x))\pi^+(x)\right]\\
&\quad - \left[(\partial_\nu - ieA_\nu(x))\pi^-(x)\right]\left[(\partial_\mu + ieA_\mu(x))\pi^+(x)\right]\\
&\quad + \frac{1}{2}\pi^0(x)\partial_\mu\partial_\nu\pi^0(x) + \frac{1}{2}(\partial_\mu\partial_\nu\pi^0(x))\pi^0(x) - (\partial_\mu\pi_0(x))(\partial_\nu\pi_0(x))\Bigg\}.
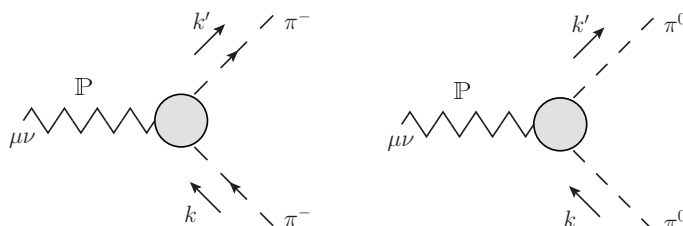\end{aligned}$$
$$\text{(B.66)}$$

The $\gamma\pi\pi$, $\gamma\gamma\pi\pi$, $\mathbb{P}\pi\pi$, and $\mathbb{P}\gamma\pi\pi$ vertices following from (B.66), including a form factor for the pomeron coupling, read as follows:

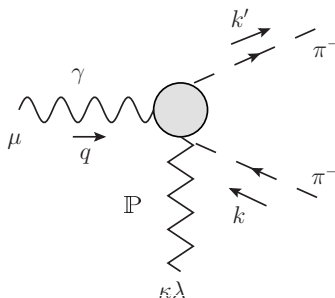$$i\Gamma_\mu^{(\gamma\pi\pi)}(k',k) = i\,e\,(k'+k)_\mu\,, \tag{B.67}$$

$$i\Gamma_{\mu\nu}^{(\gamma\gamma\pi\pi)}(k',k) = 2\,i\,e^2 g_{\mu\nu}\,, \tag{B.68}$$
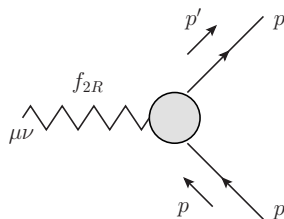

$$i\Gamma_{\mu\nu}^{(\mathbb{P}\pi\pi)}(k',k) = -i\,2\beta_{\mathbb{P}\pi\pi}F_M[(k'-k)^2]\left[(k'+k)_\mu(k'+k)_\nu - \frac{1}{4}\,g_{\mu\nu}(k'+k)^2\right]\,, \tag{B.69}$$

$$\beta_{\mathbb{P}\pi\pi} = 1.76\,\mathrm{GeV}^{-1}\,, \tag{B.70}$$

$$i\Gamma_{\mu\kappa\lambda}^{(\mathbb{P}\gamma\pi\pi)}(q,k',k) = -\,2\,i\,e\,\beta_{\mathbb{P}\pi\pi}\left[2g_{\kappa\mu}(k'+k)_\lambda + 2g_{\lambda\mu}(k'+k)_\kappa - g_{\kappa\lambda}(k'+k)_\mu\right]$$
$$\times F_M[(k'-q-k)^2]\,. \tag{B.71}$$

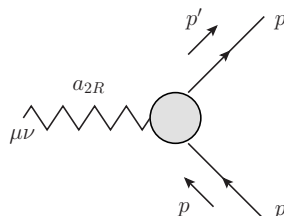- $f_{2R}pp$ (see (3.49), (3.50), and section 6.3 of [28]):

$$i\Gamma_{\mu\nu}^{(f_{2R}pp)}(p',p) = -ig_{f_{2R}pp}\frac{1}{M_0}F_1[(p'-p)^2]$$

$$\times\left\{\frac{1}{2}[\gamma_\mu(p'+p)_\nu+\gamma_\nu(p'+p)_\mu]-\frac{1}{4}g_{\mu\nu}(p\!\!\!/'+p\!\!\!/)\right\}, \tag{B.72}$$

$$g_{f_{2R}pp} = 11.04. \tag{B.73}$$

- $a_{2R}pp$ (see (3.51), (3.52), and section 6.3 of [28]):

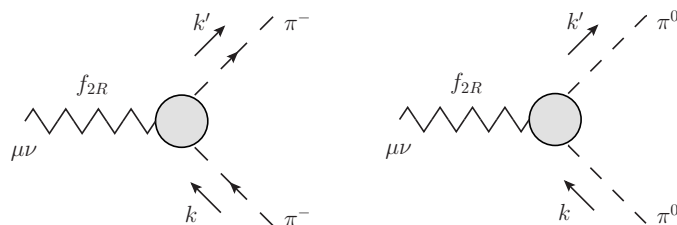$$i\Gamma_{\mu\nu}^{(a_{2R}pp)}(p',p) = -ig_{a_{2R}pp}\frac{1}{M_0}F_1[(p'-p)^2]$$

$$\times\left\{\frac{1}{2}[\gamma_\mu(p'+p)_\nu+\gamma_\nu(p'+p)_\mu]-\frac{1}{4}g_{\mu\nu}(p\!\!\!/'+p\!\!\!/)\right\}, \tag{B.74}$$

$$g_{a_{2R}pp} = 1.68. \tag{B.75}$$

- $f_{2R}\pi\pi$, $f_{2R}\gamma\pi\pi$: The vertex for $f_{2R}\pi\pi$ is given in (3.53), (3.54), and section 7.1 of [28]. The inclusion of the coupling to the photon is done by minimal substitution in complete analogy to (B.66). We get, therefore,

$$i\Gamma_{\mu\nu}^{(f_{2R}\pi\pi)}(k',k) = -i\frac{g_{f_{2R}\pi\pi}}{2M_0}F_M[(k'-k)^2]\left[(k'+k)_\mu(k'+k)_\nu-\frac{1}{4}g_{\mu\nu}(k'+k)^2\right], \tag{B.76}$$

$$g_{f_{2R}\pi\pi} = 9.30, \tag{B.77}$$
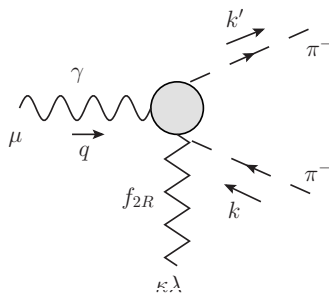
$$i\Gamma^{(f_{2R}\gamma\pi\pi)}_{\mu\kappa\lambda}(q,k',k) = -\,i\,e\frac{g_{f_{2R}\pi\pi}}{2M_0}F_M[(k'-q-k)^2] \tag{B.78}$$
$$\times\left[2g_{\kappa\mu}(k'+k)_\lambda + 2g_{\lambda\mu}(k'+k)_\kappa - g_{\kappa\lambda}(k'+k)_\mu\right].$$
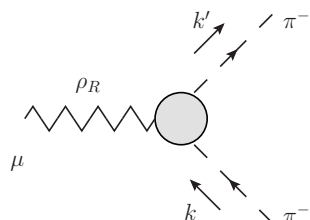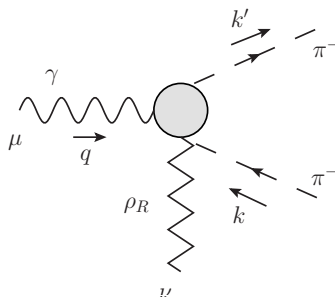
- $\rho_R\pi\pi$, $\rho_R\gamma\pi\pi$: The vertex for $\rho_R\pi\pi$ is given in (3.63), (3.64) and section 7.1 of [28]. The vertex for $\rho_R\gamma\pi\pi$ is obtained from $\rho_R\pi\pi$ by the minimal substitution rule. This gives

$$i\Gamma^{(\rho_R\pi\pi)}_\mu(k',k) = \frac{i}{2}g_{\rho_R\pi\pi}F_M[(k'-k)^2](k'+k)_\mu\,, \tag{B.79}$$

$$g_{\rho_R\pi\pi} = 15.63\,, \tag{B.80}$$

$$i\Gamma^{(\rho_R\gamma\pi\pi)}_{\mu\nu}(q,k',k) = i\,e\,g_{\rho_R\pi\pi}F_M[(k'-q-k)^2]g_{\mu\nu}\,. \tag{B.81}$$

- $\mathbb{P}\rho\rho$ (see (3.47), (3.48), and section 7.2 of [28]):
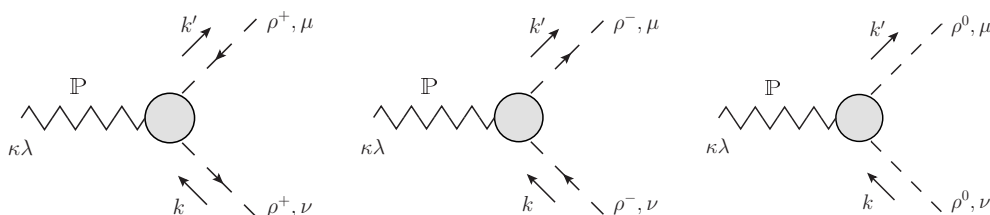
$$i\Gamma^{(\mathbb{P}\rho\rho)}_{\mu\nu\kappa\lambda}(k',k) = iF_M[(k'-k)^2]\tilde{F}^{(\rho)}(k'^2)\tilde{F}^{(\rho)}(k^2)$$
$$\times\left[2a_{\mathbb{P}\rho\rho}\Gamma^{(0)}_{\mu\nu\kappa\lambda}(k',-k) - b_{\mathbb{P}\rho\rho}\Gamma^{(2)}_{\mu\nu\kappa\lambda}(k',-k)\right]\,, \tag{B.82}$$

$$a_{\mathbb{P}\rho\rho} \geq 0\,,$$
$$2m_\rho^2 a_{\mathbb{P}\rho\rho} + b_{\mathbb{P}\rho\rho} \geq 0\,. \tag{B.83}$$

In section 7.2 of [28] arguments for the following relation were presented:

$$2m_\rho^2 a_{\mathbb{P}\rho\rho} + b_{\mathbb{P}\rho\rho} = 4\beta_{\mathbb{P}\pi\pi} = 7.04\,\text{GeV}^{-1}\,. \tag{B.84}$$

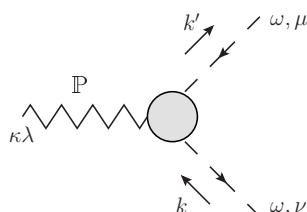This should be considered as a default relation to be checked and, if necessary, corrected by experiment. In (B.82) we have introduced form factors $\tilde{F}^{(\rho)}$ which can take into account that off-shell ρ mesons need not have the same coupling to the pomeron as "on-shell" ρ mesons. A convenient form for $\tilde{F}^{(\rho)}$ is

$$\tilde{F}^{(\rho)}(k^2) = \left[1 + \frac{k^2(k^2 - m_\rho^2)}{\Lambda_\rho^4} \right]^{-n_\rho} \tag{B.85}$$

with Λ_ρ a parameter in the range 2 to 5 GeV and $n_\rho > 0$. Here we have

$$\tilde{F}^{(\rho)}(0) = \tilde{F}^{(\rho)}(m_\rho^2) = 1 \,. \tag{B.86}$$

• $\mathbb{P}\omega\omega$:

$$i\Gamma_{\mu\nu\kappa\lambda}^{(\mathbb{P}\omega\omega)}(k', k) = i\, F_M[(k' - k)^2]\tilde{F}^{(\omega)}(k'^2)\tilde{F}^{(\omega)}(k^2)$$
$$\times \left[2a_{\mathbb{P}\omega\omega}\Gamma_{\mu\nu\kappa\lambda}^{(0)}(k', -k) - b_{\mathbb{P}\omega\omega}\Gamma_{\mu\nu\kappa\lambda}^{(2)}(k', -k) \right] \,. \tag{B.87}$$

As default values we may choose here

$$a_{\mathbb{P}\omega\omega} = a_{\mathbb{P}\rho\rho} \,,$$
$$b_{\mathbb{P}\omega\omega} = b_{\mathbb{P}\rho\rho} \,, \tag{B.88}$$
$$\tilde{F}^{(\omega)}(k^2) = \tilde{F}^{(\rho)}(k^2) \,.$$

• $\mathbb{P}\rho'\rho'$: Here our ansatz reads as for $\mathbb{P}\rho\rho$ (B.82) with ρ replaced by ρ'. We have no good estimates for the values of the $\mathbb{P}\rho'\rho'$ parameters. Thus, reasonable default values are again the $\mathbb{P}\rho\rho$ parameters

$$a_{\mathbb{P}\rho'\rho'} = a_{\mathbb{P}\rho\rho} \,,$$
$$b_{\mathbb{P}\rho'\rho'} = b_{\mathbb{P}\rho\rho} \,, \tag{B.89}$$
$$\tilde{F}^{(\rho')}(k^2) = \tilde{F}^{(\rho)}(k^2) \,.$$

• $f_{2R}\rho\rho$, $f_{2R}\omega\omega$, $f_{2R}\rho'\rho'$ (see (3.55), (3.56), and section 7.2 of [28]):
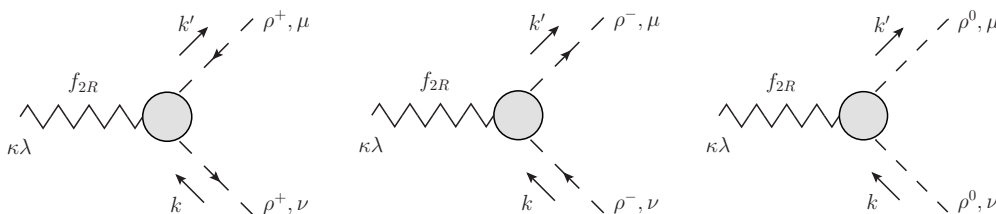
$$i\Gamma^{(f_{2R}\rho\rho)}_{\mu\nu\kappa\lambda}(k',k) = iF_M[(k'-k)^2]\tilde{F}^{(\rho)}(k'^2)\tilde{F}^{(\rho)}(k^2)$$
$$\times \left[2a_{f_{2R}\rho\rho}\Gamma^{(0)}_{\mu\nu\kappa\lambda}(k',-k) - b_{f_{2R}\rho\rho}\Gamma^{(2)}_{\mu\nu\kappa\lambda}(k',-k) \right], \quad \text{(B.90)}$$

$$a_{f_{2R}\rho\rho} = 2.92\,\text{GeV}^{-3}, \qquad b_{f_{2R}\rho\rho} = 5.02\,\text{GeV}^{-1}. \quad \text{(B.91)}$$

For the $f_{2R}\omega\omega$ and the $f_{2R}\rho'\rho'$ couplings our ansatz is as for $f_{2R}\rho\rho$ but with parameters $a_{f_{2R}\omega\omega}$, $b_{f_{2R}\omega\omega}$ and $a_{f_{2R}\rho'\rho'}$, $b_{f_{2R}\rho'\rho'}$, respectively. For the ω we have, of course, only the analogue of the rightmost of the above diagrams. For lack of other information we set as default

$$a_{f_{2R}\omega\omega} = a_{f_{2R}\rho'\rho'} = a_{f_{2R}\rho\rho},$$
$$b_{f_{2R}\omega\omega} = b_{f_{2R}\rho'\rho'} = b_{f_{2R}\rho\rho}. \quad \text{(B.92)}$$

- $a_{2R}\omega\rho$ (see (3.57), (3.58), and section 7.2 of [28]):

$$i\Gamma^{(a_{2R}\omega\rho)}_{\mu\nu\kappa\lambda}(k',k) = iF_M[(k'-k)^2]\tilde{F}^{(\rho)}(k'^2)\tilde{F}^{(\omega)}(k^2)$$
$$\times \left[2a_{a_{2R}\omega\rho}\Gamma^{(0)}_{\mu\nu\kappa\lambda}(k',-k) - b_{a_{2R}\omega\rho}\Gamma^{(2)}_{\mu\nu\kappa\lambda}(k',-k) \right], \quad \text{(B.93)}$$

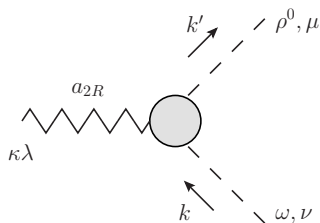$$|a_{a_{2R}\omega\rho}| = 2.56\,\text{GeV}^{-3}, \qquad |b_{a_{2R}\omega\rho}| = 4.68\,\text{GeV}^{-1}. \quad \text{(B.94)}$$

- $\omega_R pp$ (see (3.59), (3.60), and section 6.3 of [28]):
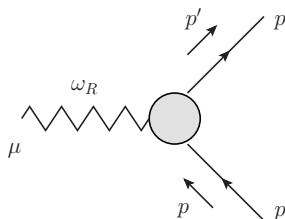
$$i\Gamma^{(\omega_R pp)}_\mu(p',p) = -ig_{\omega_R pp}F_1[(p'-p)^2]\gamma_\mu, \quad \text{(B.95)}$$

$$g_{\omega_R pp} = 8.65. \quad \text{(B.96)}$$

- $\rho_R pp$ (see (3.61), (3.62), and section 6.3 of [28]):

$$i\Gamma_{\mu}^{(\rho_R pp)}(p',p) = -ig_{\rho_R pp}F_1[(p'-p)^2]\gamma_{\mu}\,, \tag{B.97}$$

$$g_{\rho_R pp} = 2.02\,. \tag{B.98}$$

- $\rho_R\rho f_2$ (see (3.66), (3.67), and section 7.2 of [28]):
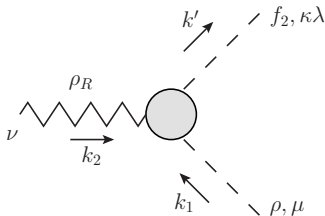
$$i\Gamma_{\mu\nu\kappa\lambda}^{(\rho_R\rho f_2)}(k',k_1) = iF_M(k_2^2)F^{(f_2\pi\pi)}(k'^2)\tilde{F}^{(\rho)}(k_1^2)$$
$$\times \left[2a_{\rho_R\rho f_2}\Gamma_{\mu\nu\kappa\lambda}^{(0)}(k_1,k_2) - b_{\rho_R\rho f_2}\Gamma_{\mu\nu\kappa\lambda}^{(2)}(k_1,k_2)\right]\,, \tag{B.99}$$

where $k' = k_1 + k_2$ and

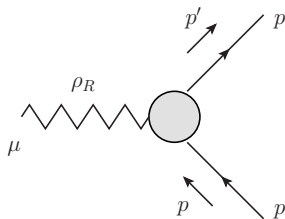$$a_{\rho_R\rho f_2} = 2.92\,\text{GeV}^{-3}\,, \qquad b_{\rho_R\rho f_2} = 5.02\,\text{GeV}^{-1}\,. \tag{B.100}$$

- $\omega_R\omega f_2$ (see (3.65) and section 7.2 of [28]):
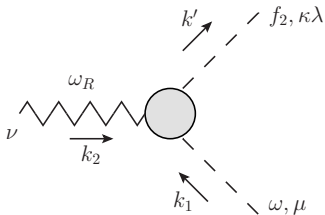
$$i\Gamma_{\mu\nu\kappa\lambda}^{(\omega_R\omega f_2)}(k',k_1) = iF_M(k_2^2)F^{(f_2\pi\pi)}(k'^2)\tilde{F}^{(\omega)}(k_1^2)$$
$$\times \left[2a_{\omega_R\omega f_2}\Gamma_{\mu\nu\kappa\lambda}^{(0)}(k_1,k_2) - b_{\omega_R\omega f_2}\Gamma_{\mu\nu\kappa\lambda}^{(2)}(k_1,k_2)\right] \tag{B.101}$$

with $k' = k_1 + k_2$. As default values we choose according to (7.31) to (7.36) of [28]

$$a_{\omega_R\omega f_2} = a_{\rho_R\rho f_2} = 2.92\,\text{GeV}^{-3}\,, \tag{B.102}$$
$$b_{\omega_R\omega f_2} = b_{\rho_R\rho f_2} = 5.02\,\text{GeV}^{-1}\,.$$

- $\mathbb{O}pp$ (see (3.68), (3.69), and section 6.2 of [28]):
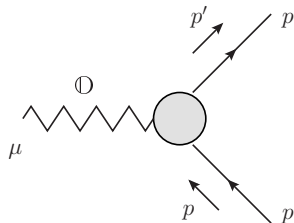
$$i\Gamma_{\mu}^{(\mathbb{O}pp)}(p',p) = -i\,3\,\beta_{\mathbb{O}pp}M_0F_1[(p'-p)^2]\gamma_{\mu}\,. \tag{B.103}$$

The coupling parameter $\beta_{\mathbb{O}pp}$ has dimension GeV^{-1}.

- $\mathbb{O}\gamma f_2$ (see (3.70), (3.71), and section 6.2 of [28]):
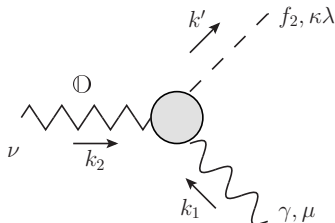
$$i\Gamma^{(\mathbb{O}\gamma f_2)}_{\mu\nu\kappa\lambda}(k', k_1) = iF_M(k_1^2)F_M(k_2^2)F^{(f_2\pi\pi)}(k'^2)$$
$$\times \left[2a_{\mathbb{O}\gamma f_2}\Gamma^{(0)}_{\mu\nu\kappa\lambda}(k_1, k_2) - b_{\mathbb{O}\gamma f_2}\Gamma^{(2)}_{\mu\nu\kappa\lambda}(k_1, k_2) \right] \quad \text{(B.104)}$$

with $k' = k_1 + k_2$ and

$$a_{\mathbb{O}\gamma f_2} = e\hat{a}_{\mathbb{O}\gamma f_2}, \qquad b_{\mathbb{O}\gamma f_2} = e\hat{b}_{\mathbb{O}\gamma f_2}. \quad \text{(B.105)}$$

Here $\hat{a}_{\mathbb{O}\gamma f_2}$ and $\hat{b}_{\mathbb{O}\gamma f_2}$ are (unknown) odderon coupling parameters of hadronic scale with dimensions GeV^{-3} and GeV^{-1}, respectively.

In table 1 we list all parameters of the model, the corresponding equations and references. For many parameters the default values given are rather well constrained from other sources as indicated. For parameters where there is an asterisk $*$ in the last column we have no good estimates. The default values quoted there are just educated guesses used to produce plots for the cross sections and asymmetries shown in section 3.

C Behaviour of $C = -1$ exchanges for $t \to 0$

Consider the reaction (1.1) in the $\pi^+\pi^-$ rest frame using the proton-Jackson system; see appendix A, figure 10. We have then from (A.9)

$$p^0 = \frac{1}{m_{\pi^+\pi^-}}(p \cdot k) = \frac{1}{2m_{\pi^+\pi^-}}(s - m_p^2 + t),$$
$$p'^0 = \frac{1}{m_{\pi^+\pi^-}}(p' \cdot k) = \frac{1}{2m_{\pi^+\pi^-}}(s - m_p^2 - m_{\pi^+\pi^-}^2),$$
$$p^0 - p'^0 = \frac{1}{2m_{\pi^+\pi^-}}(m_{\pi^+\pi^-}^2 + t). \quad \text{(C.1)}$$

For $s = W_{\gamma p}^2 \gg m_{\pi^+\pi^-}^2, m_p^2, |t|$ we get, neglecting terms of relative order $m_{\pi^+\pi^-}^2/s$, m_p^2/s, $|t|/s$, the following:

$$p + p' = \begin{pmatrix} p^0 + p'^0 \\ \mathbf{p}'_\perp \\ p^0 + p'^0 \end{pmatrix}, \qquad p - p' = \begin{pmatrix} p^0 - p'^0 \\ -\mathbf{p}'_\perp \\ p^0 - p'^0 \end{pmatrix}, \quad \text{(C.2)}$$

$$p + p' \cong \frac{p^0 + p'^0}{p^0 - p'^0}(p - p') + \frac{2p^0}{p^0 - p'^0}\begin{pmatrix} 0 \\ \mathbf{p}'_\perp \\ 0 \end{pmatrix}. \quad \text{(C.3)}$$

Now the γpp vertex in the diagram for the Primakoff contribution, see figure 1(c), gives at high energies a factor $(p + p')$, the emitted virtual photon has momentum $p - p'$ and it is nearly real for $|t| \to 0$. Gauge invariance at the $f_2 \gamma \gamma$ vertex implies then that the first term on the r.h.s. of (C.3) does not contribute. Thus, for $|t| \to 0$ the nearly real photon has effectively transverse linear polarisation due to the second term on the r.h.s. of (C.3). From this argument we expect to get a factor $\mathbf{p}'_\perp$ in the amplitude and a factor $|\mathbf{p}'_\perp|^2 \cong |t|$ in the cross section. For the Primakoff effect we get also a factor $1/|t|^2$ from the photon propagator leaving us with a behaviour of $d\sigma/dt \propto 1/|t|$ for small $|t|$. The reggeon and the odderon contributions from figures 1(b) and 1(d), respectively, behave as $d\sigma/dt \propto |t|$ for $|t| \to 0$ since the effective propagators have no singularity there.

D   Determination of the Monte Carlo weights

In this appendix relevant formulae for the weight determination in the event generator are listed. The fivefold differential cross section of the reaction (1.1) is given by the product of a normalisation term, the spin-sum of all matrix elements discussed above and the three-body differential phase space element $d\phi_3$,

$$d\sigma^{\gamma p} = \frac{1}{4} \frac{1}{2(s - m_p^2)} (\hbar c)^2 \left((-1) \sum_{\mathfrak{s}', \mathfrak{s}} \mathcal{M}^*_{\mu, \mathfrak{s}', \mathfrak{s}} \mathcal{M}^\mu_{\mathfrak{s}', \mathfrak{s}} \right) d\phi_3 \,, \tag{D.1}$$

$$d\phi_3 = \frac{1}{(2\pi)^5} \frac{d^3 k_1}{2k_1^0} \frac{d^3 k_2}{2k_2^0} \frac{d^3 p'}{2p'^0} \delta^{(4)}(k_1 + k_2 + p' - p - q) \,, \tag{D.2}$$

where the conversion constant $(\hbar c)^2$ is written out explicitly.

In this appendix we use the notation

$$m_{\pi\pi} \equiv m_{\pi^+\pi^-} \,, \qquad m_q = 0 \,, \qquad t_2 = (q - k_2)^2 \,. \tag{D.3}$$

For our model it is convenient to express the three-body phase space element as

$$d\phi_3 = \frac{1}{(2\pi)^5} \frac{1}{8} \frac{1}{2m_{\pi\pi}} \frac{\lambda^{1/2}(m_{\pi\pi}^2, m_\pi^2, m_\pi^2)}{\lambda^{1/2}(s, m_p^2, m_q^2)} \, dm_{\pi\pi} \, dt \, d\varphi_p \, d\cos\vartheta_{\pi_2} \, d\varphi_{\pi_2} \tag{D.4}$$

with

$$\lambda(x, y, z) = x^2 - 2(y + z)x + (y - z)^2 \,, \tag{D.5}$$

and with φ_p being the azimuthal angle of the outgoing proton in the γp rest-frame, and ϑ_{π_2} and φ_{π_2} being the angles of one π in the $\pi^+\pi^-$ rest-frame. Furthermore the conditions for the physically accessible region must be taken into account, compare with [67], p. 89 and p. 131,

$$G(s, t, m_{\pi\pi}^2, m_p^2, m_q^2, m_{p'}^2) \leq 0 \qquad \text{and}$$
$$G(m_{\pi\pi}^2, t_2, m_\pi^2, t, m_p^2, m_\pi^2) \leq 0 \tag{D.6}$$

with

$$\begin{aligned} G(x, y, z, u, v, w) = {} & x^2 y + x y^2 + z^2 u + z u^2 + v^2 w + v w^2 + xzw + xuv \\ & + yzw + yuw - xy(z + u + v + w) \\ & - zu(x + y + v + w) - vw(x + y + z + u) \,. \end{aligned} \tag{D.7}$$

Parameters	See eqs.	Default value	Constraint	Ref.	
m_ρ	(B.3)–(B.18)	$775.26\,\mathrm{MeV}$	$775.26 \pm 0.25\,\mathrm{MeV}$	[69]	
m_ω	(B.3)–(B.18)	$782.65\,\mathrm{MeV}$	$782.65 \pm 0.12\,\mathrm{MeV}$	[69]	
Γ_ω	(B.3)–(B.18)	$8.49\,\mathrm{MeV}$	$8.49 \pm 0.08\,\mathrm{MeV}$	[69]	
$b_{\rho\omega}$	(B.17)	3.5×10^{-3}	$(3.5 \pm 0.5) \times 10^{-3}$	[68]	
$g_{\rho\pi\pi}$	(B.17), (B.56)	11.51	11.51 ± 0.07	[68]	
$g_{\omega\pi\pi}$	(B.17), (B.57)	-0.35	-0.35 ± 0.10	[68]	
$m_{\rho'}$	(B.22)	$1465\,\mathrm{MeV}$	$1465 \pm 25\,\mathrm{MeV}$	[69]	
$\Gamma_{\rho'}$	(B.22)	$400\,\mathrm{MeV}$	$400 \pm 60\,\mathrm{MeV}$	[69]	
$g_{\rho'\pi\pi}$	(B.55)	0.5			*
m_{f_2}	(B.29)	$1275.1\,\mathrm{MeV}$	$1275.1 \pm 1.2\,\mathrm{MeV}$	[69]	
Γ_{f_2}	(B.29)	$185.1\,\mathrm{MeV}$	$185.1^{+2.9}_{-2.4}\,\mathrm{MeV}$	[69]	
$\frac{\Gamma(f_2 \to \pi\pi)}{\Gamma_{f_2}}$	(B.30)	84.8%	$(84.8^{+2.4}_{-1.2})\%$	[69]	
$\epsilon_{\mathbb{P}}$	(B.32)	0.0808	0.0808	[28]	
$\alpha'_{\mathbb{P}}$	(B.32)	$0.25\,\mathrm{GeV}^{-2}$	$0.25\,\mathrm{GeV}^{-2}$	[28]	
$\alpha_{\mathbb{R}_+}(0)$	(B.34)	0.5475	0.5475	[28]	
$\alpha'_{\mathbb{R}_+}$	(B.34)	$0.9\,\mathrm{GeV}^{-2}$	$0.9\,\mathrm{GeV}^{-2}$	[28]	
$\alpha_{\mathbb{R}_-}(0)$	(B.36)	0.5475	0.5475	[28]	
$\alpha'_{\mathbb{R}_-}$	(B.36)	$0.9\,\mathrm{GeV}^{-2}$	$0.9\,\mathrm{GeV}^{-2}$	[28]	
M_-	(B.36)	$1.41\,\mathrm{GeV}$	$1.41\,\mathrm{GeV}$	[28]	
$\eta_{\mathbb{O}}$	(B.38)	-1	± 1	[28]	*
$\epsilon_{\mathbb{O}}$	(B.38)	0	$\epsilon_{\mathbb{O}} \leq \epsilon_{\mathbb{P}}$	[28]	*
$\alpha'_{\mathbb{O}}$	(B.38)	0.25		[28]	*
γ_ρ	(B.46)	$\left[\frac{1}{4\pi}0.496\right]^{-1/2}$	$\left[\frac{1}{4\pi}(0.496 \pm 0.023)\right]^{-1/2}$	[28]	
γ_ω	(B.46)	$\left[\frac{1}{4\pi}0.042\right]^{-1/2}$	$\left[\frac{1}{4\pi}(0.042 \pm 0.0015)\right]^{-1/2}$	[28]	
γ_ϕ	(B.46)	$-\left[\frac{1}{4\pi}0.0716\right]^{-1/2}$	$-\left[\frac{1}{4\pi}(0.0716 \pm 0.0017)\right]^{-1/2}$	[28]	
$\gamma_{\rho'}$	(B.46)	γ_ρ			*
$\frac{\mu_p}{\mu_N}$	(B.52)	2.7928	2.7928	[28]	
m_D^2	(B.53)	$0.71\,\mathrm{GeV}^2$	$0.71\,\mathrm{GeV}^2$	[28]	
m_0^2	(B.54)	$0.50\,\mathrm{GeV}^2$	$0.50\,\mathrm{GeV}^2$	[28]	
$g_{f_2\pi\pi}$	(B.59)	9.26	9.26 ± 0.15	[28]	
Λ_{f_2}	(B.60)	$1.8\,\mathrm{GeV}$	$1 - 4\,\mathrm{GeV}$		*
$a_{f_2\gamma\gamma}$	(B.62)	$\frac{e^2}{4\pi}1.45\,\mathrm{GeV}^{-3}$	$\frac{e^2}{4\pi}1.45\,\mathrm{GeV}^{-3}$	[28]	
$b_{f_2\gamma\gamma}$	(B.62)	$\frac{e^2}{4\pi}2.49\,\mathrm{GeV}^{-1}$	$\frac{e^2}{4\pi}2.49\,\mathrm{GeV}^{-1}$	[28]	
$\beta_{\mathbb{P}NN}$	(B.65)	$1.87\,\mathrm{GeV}^{-1}$	$1.87\,\mathrm{GeV}^{-1}$	[28]	
$\beta_{\mathbb{P}\pi\pi}$	(B.70)	$1.76\,\mathrm{GeV}^{-1}$	$1.76\,\mathrm{GeV}^{-1}$	[28]	
g_{f_2Rpp}	(B.73)	11.04	11.04	[28]	
g_{a_2Rpp}	(B.75)	1.68	1.68	[28]	

Table 1. Continued on next page

$g_{f_{2R}\pi\pi}$	(B.77)	9.30	9.30	[28]	
$g_{\rho_R\pi\pi}$	(B.80)	15.63	15.63	[28]	
$a_{\mathbb{P}\rho\rho}$	(B.82), (B.83)	$0.45\,\text{GeV}^{-3}$		[28]	$*$
$b_{\mathbb{P}\rho\rho}$	(B.82), (B.83)	$6.5\,\text{GeV}^{-1}$		[28]	$*$
$2m_\rho^2 a_{\mathbb{P}\rho\rho} + b_{\mathbb{P}\rho\rho}$	(B.84)	$7.04\,\text{GeV}^{-1}$	$7.04\,\text{GeV}^{-1}$	[28]	
Λ_ρ	(B.85)	$2\,\text{GeV}$	$2-5\,\text{GeV}$		$*$
n_ρ	(B.85)	0.4	$n_\rho > 0$		$*$
Λ_ω	(B.88)	$2\,\text{GeV}$	$2-5\,\text{GeV}$		$*$
n_ω	(B.88)	0.4	$n_\omega > 0$		$*$
$\Lambda_{\rho'}$	(B.89)	$2\,\text{GeV}$	$2-5\,\text{GeV}$		$*$
$n_{\rho'}$	(B.89)	0.4	$n_{\rho'} > 0$		$*$
$a_{\mathbb{P}\omega\omega}$	(B.88)	$0.45\,\text{GeV}^{-3}$			$*$
$b_{\mathbb{P}\omega\omega}$	(B.88)	$6.5\,\text{GeV}^{-1}$			$*$
$a_{\mathbb{P}\rho'\rho'}$	(B.89)	$0.45\,\text{GeV}^{-3}$			$*$
$b_{\mathbb{P}\rho'\rho'}$	(B.89)	$6.5\,\text{GeV}^{-1}$			$*$
$a_{f_{2R}\rho\rho}$	(B.91)	$2.92\,\text{GeV}^{-3}$	$2.92\,\text{GeV}^{-3}$	[28]	
$b_{f_{2R}\rho\rho}$	(B.91)	$5.02\,\text{GeV}^{-1}$	$5.02\,\text{GeV}^{-1}$	[28]	
$a_{f_{2R}\omega\omega}$	(B.92)	$2.92\,\text{GeV}^{-3}$			$*$
$b_{f_{2R}\omega\omega}$	(B.92)	$5.02\,\text{GeV}^{-1}$			$*$
$a_{f_{2R}\rho'\rho'}$	(B.92)	$2.92\,\text{GeV}^{-3}$			$*$
$b_{f_{2R}\rho'\rho'}$	(B.92)	$5.02\,\text{GeV}^{-1}$			$*$
$a_{a_{2R}\omega\rho}$	(B.94)	$+2.56\,\text{GeV}^{-3}$	$\pm 2.56\,\text{GeV}^{-3}$	[28]	
$b_{a_{2R}\omega\rho}$	(B.94)	$+4.68\,\text{GeV}^{-1}$	$\pm 4.68\,\text{GeV}^{-1}$	[28]	
$g_{\omega_R pp}$	(B.96)	8.65	8.65	[28]	
$g_{\rho_R pp}$	(B.98)	2.02	2.02	[28]	
$a_{\rho_R\rho f_2}$	(B.100)	$2.92\,\text{GeV}^{-3}$	$2.92\,\text{GeV}^{-3}$	[28]	
$b_{\rho_R\rho f_2}$	(B.100)	$5.02\,\text{GeV}^{-1}$	$5.02\,\text{GeV}^{-1}$	[28]	
$a_{\omega_R\omega f_2}$	(B.102)	$2.92\,\text{GeV}^{-3}$	$2.92\,\text{GeV}^{-3}$	[28]	
$b_{\omega_R\omega f_2}$	(B.102)	$5.02\,\text{GeV}^{-1}$	$5.02\,\text{GeV}^{-1}$	[28]	
$\beta_{\mathbb{O}pp}$	(B.103)	$0.18\,\text{GeV}^{-1}$		[28]	$*$
$\hat{a}_{\mathbb{O}\gamma f_2}$	(B.104), (B.105)	$0.5\,\text{GeV}^{-3}$		[28]	$*$
$\hat{b}_{\mathbb{O}\gamma f_2}$	(B.104), (B.105)	$0.5\,\text{GeV}^{-1}$		[28]	$*$
M_0		$\equiv 1\,\text{GeV}$			

Table 1. The parameters and their default values for the model. An asterisk $*$ in the last column means that we have no good estimate in this case. For most of the parameters constraints from experiment or theory are available, for all other parameters example values are chosen. The listed default values are used to produce the cross section and asymmetry plots in section 3. The references given are only meant to indicate where a complete discussion of the parameter in question, with appropriate references, can be found. The parameter $M_0 \equiv 1\,\text{GeV}$ is introduced for dimensional reasons in various equations.

The γp cross section in the ranges $\Delta m_{\pi\pi} = [m_{\pi\pi,\,\min}, m_{\pi\pi,\,\max}]$ and $\Delta t = [t_{\min}, t_{\max}]$ is obtained by integrating over $m_{\pi\pi}$, t and all angles:

$$\sigma^{\gamma p}(\Delta m_{\pi\pi}, \Delta t) = \int\limits_{\Delta m_{\pi\pi}} \int\limits_{\Delta t} \int\limits_{\text{angles}} d\sigma^{\gamma p} \tag{D.8}$$

$$= \int\limits_{\Delta m_{\pi\pi}} \int\limits_{\Delta t} \int\limits_{\text{angles}} \frac{1}{4} \frac{1}{2(s - m_p^2)} (\hbar c)^2$$

$$\times |\mathcal{M}(m_{\pi\pi}, t, \cos\vartheta_{\pi_2}, \varphi_{\pi_2})|^2$$

$$\times \frac{1}{(2\pi)^5} \frac{1}{8} \frac{1}{2m_{\pi\pi}} \frac{\lambda^{1/2}(m_{\pi\pi}^2, m_\pi^2, m_\pi^2)}{\lambda^{1/2}(s, m_p^2, m_q^2)}$$

$$\times \theta\big(-G(s, t, m_{\pi\pi}^2, m_p^2, m_q^2, t)\big)$$

$$\times \theta\big(-G(m_{\pi\pi}^2, t_2, m_\pi^2, t, m_p^2, m_\pi^2)\big)$$

$$\times dm_{\pi\pi}\, dt\, d\varphi_p\, d\cos\vartheta_{\pi_2}\, d\varphi_{\pi_2}\,,$$

with $|\mathcal{M}(m_{\pi\pi}, t, \cos\vartheta_{\pi_2}, \varphi_{\pi_2})|^2 = (-1) \sum_{s,s'} \mathcal{M}^*_{\mu,s',s} \mathcal{M}^\mu_{s',s}$ and using the equations (D.1)–(D.7). With Monte Carlo importance sampling this integral can be approximated by

$$\sigma^{\gamma p}(\Delta m_{\pi\pi}, \Delta t) \approx \frac{1}{N} \sum_{i=0}^{N} \frac{1}{g(m_{\pi\pi,i}, t_i, \varphi_{p,i}, \vartheta_{\pi_2,i}, \varphi_{\pi_2,i})} \tag{D.9}$$

$$\times \frac{1}{4} \frac{1}{2(s - m_p^2)} (\hbar c)^2$$

$$\times |\mathcal{M}(m_{\pi\pi,i}, t_i, \cos\vartheta_{\pi_2,i}, \varphi_{\pi_2,i})|^2$$

$$\times \frac{1}{(2\pi)^5} \frac{1}{8} \frac{1}{2\, m_{\pi\pi_i}} \frac{\lambda^{1/2}(m_{\pi\pi,i}^2, m_\pi^2, m_\pi^2)}{\lambda^{1/2}(s, m_p^2, m_q^2)}$$

$$\times \theta\left(-G(s, t_i, m_{\pi\pi,i}^2, m_p^2, m_q^2, t_i)\right)$$

$$\times \theta\left(-G(m_{\pi\pi,i}^2, t_{2,i}, m_\pi^2, t_i, m_p^2, m_\pi^2)\right)\,,$$

with N kinematic points $x_i = [m_{\pi\pi,i}, t_i, \varphi_{p,i}, \cos\vartheta_{\pi_2,i}, \varphi_{\pi_2,i}]$ randomly chosen according to a suitable pre-sampling density distribution $g(m_{\pi\pi}, t, \varphi_p, \vartheta_{\pi_2}, \varphi_{\pi_2})$. The event weight w_i of a randomly chosen event i is then given by the product of all terms with index i in the sum on the r. h. s. of (D.9) divided by N, such that $\sigma^{\gamma p}(\Delta m_{\pi\pi}, \Delta t) \approx \sum_{i=0}^{N} w_i$.

References

[1] T.H. Bauer, R.D. Spital, D.R. Yennie and F.M. Pipkin, *The hadronic properties of the photon in high-energy interactions*, *Rev. Mod. Phys.* **50** (1978) 261 [*Erratum ibid.* **51** (1979) 407] [INSPIRE].

[2] A. Donnachie, H.G. Dosch, P.V. Landshoff and O. Nachtmann, *Pomeron physics and QCD*, Cambridge Monographs on Particle Physics, Nuclear Physics and Cosmology, volume 19, Cambridge University Press, Cambridge U.K. (2002).

[3] F.E. Close, A. Donnachie and G. Shaw, *Electromagnetic interactions and hadronic structure*, Cambridge Monographs on Particle Physics, Nuclear Physics and Cosmology, volume 25, Cambridge University Press, Cambridge U.K. (2007).

[4] R. Fiore, L.L. Jenkovszky, F. Paccanoni and A. Prokudin, *The pomeron in exclusive vector meson production*, *Phys. Rev.* **D 68** (2003) 014005 [hep-ph/0302195] [INSPIRE].

[5] A. Szczurek and A.P. Szczepaniak, *Diffractive photoproduction of opposite-charge pseudoscalar meson pairs at high energies*, *Phys. Rev.* **D 71** (2005) 054005 [hep-ph/0410083] [INSPIRE].

[6] J.R. Forshaw and R. Sandapen, *An AdS/QCD holographic wavefunction for the ρ meson and diffractive ρ meson electroproduction*, *Phys. Rev. Lett.* **109** (2012) 081601 [arXiv:1203.6088] [INSPIRE].

[7] C. Berger, N.B. Mistry, L. Roberts, R. Talman and P. Walstrom, *"Elastic" photoproduction of ρ^0 and ϕ^0 mesons from hydrogen*, *Phys. Lett.* **B 39** (1972) 659 [INSPIRE].

[8] Y. Eisenberg et al., *Study of high-energy photoproduction with positron-annihilation radiation: I. three-prong events*, *Phys. Rev.* **D 5** (1972) 15 [INSPIRE].

[9] J. Park et al., *The reaction $\gamma p \rightarrow \rho^0 p$ at $5.5\,GeV$ to $18\,GeV$*, *Nucl. Phys.* **B 36** (1972) 404 [INSPIRE].

[10] J. Ballam et al., *Bubble-chamber study of photoproduction by $2.8\,GeV$ and $4.7\,GeV$ polarized photons. I. cross-section determinations and production of ρ^0 and Δ^{++} in the reaction $\gamma p \rightarrow p\pi^+\pi^-$*, *Phys. Rev.* **D 5** (1972) 545 [INSPIRE].

[11] J. Ballam et al., *Vector-meson production by polarized photons at $2.8\,GeV$, $4.7\,GeV$ and $9.3\,GeV$*, *Phys. Rev.* **D 7** (1973) 3150 [INSPIRE].

[12] G.E. Gladding, J.J. Russell, M.J. Tannenbaum, J.M. Weiss and G.B. Thomson, *Measurement of photoproduction of ω^0 and ρ^0 mesons in hydrogen*, *Phys. Rev.* **D 8** (1973) 3721 [INSPIRE].

[13] AACHEN-HAMBURG-HEIDELBERG-MUNICH collaboration, W. Struczinski et al., *Study of photoproduction on hydrogen in a streamer chamber with tagged photons for $1.6\,GeV < E_\gamma < 6.3\,GeV$: topological and reaction cross-sections*, *Nucl. Phys.* **B 108** (1976) 45 [INSPIRE].

[14] R.M. Egloff et al., *Measurements of elastic ρ and ϕ meson photoproduction cross-sections on protons from $30\,GeV$ to $180\,GeV$*, *Phys. Rev. Lett.* **43** (1979) 657 [INSPIRE].

[15] D. Aston et al., *Photoproduction of ρ^0 and ω on hydrogen at photon energies of $20\,GeV$ to $70\,GeV$*, *Nucl. Phys.* **B 209** (1982) 56 [INSPIRE].

[16] ZEUS collaboration, M. Derrick et al., *Measurement of elastic ρ^0 photoproduction at HERA*, *Z. Phys.* **C 69** (1995) 39 [hep-ex/9507011] [INSPIRE].

[17] H1 collaboration, S. Aid et al., *Elastic photoproduction of ρ^0 mesons at HERA*, *Nucl. Phys.* **B 463** (1996) 3 [hep-ex/9601004] [INSPIRE].

[18] ZEUS collaboration, J. Breitweg et al., *Elastic and proton dissociative ρ^0 photoproduction at HERA*, *Eur. Phys. J.* **C 2** (1998) 247 [hep-ex/9712020] [INSPIRE].

[19] G. Baur, K. Hencken, D. Trautmann, S. Sadovsky and Y. Kharlov, *Coherent $\gamma\gamma$ and γA interactions in very peripheral collisions at relativistic ion colliders*, *Phys. Rept.* **364** (2002) 359 [hep-ph/0112211] [INSPIRE].

[20] C.A. Bertulani, S.R. Klein and J. Nystrand, *Physics of ultra-peripheral nuclear collisions*, *Ann. Rev. Nucl. Part. Sci.* **55** (2005) 271 [nucl-ex/0502005] [INSPIRE].

[21] A.J. Baltz et al., *The physics of ultraperipheral collisions at the LHC*, *Phys. Rept.* **458** (2008) 1 [arXiv:0706.3356] [INSPIRE].

[22] R. Staszewski, P. Lebiedowicz, M. Trzebinski, J. Chwastowski and A. Szczurek, *Exclusive $\pi^+\pi^-$ production at the LHC with forward proton tagging*, *Acta Phys. Polon.* **B 42** (2011) 1861 [arXiv:1104.3568] [INSPIRE].

[23] STAR collaboration, C. Adler et al., *Coherent ρ^0 production in ultraperipheral heavy ion collisions*, *Phys. Rev. Lett.* **89** (2002) 272302 [nucl-ex/0206004] [INSPIRE].

[24] STAR collaboration, B.I. Abelev et al., *ρ^0 photoproduction in ultraperipheral relativistic heavy ion collisions at $\sqrt{s_{NN}} = 200\,GeV$*, *Phys. Rev.* **C 77** (2008) 034910 [arXiv:0712.3320] [INSPIRE].

[25] STAR collaboration, B.I. Abelev et al., *Observation of two-source interference in the photoproduction reaction $Au\,Au \to Au\,Au\,\rho^0$*, *Phys. Rev. Lett.* **102** (2009) 112301 [arXiv:0812.1063] [INSPIRE].

[26] STAR collaboration, G. Agakishiev et al., *ρ^0 photoproduction in AuAu collisions at $\sqrt{s_{NN}} = 62.4\,GeV$ with STAR*, *Phys. Rev.* **C 85** (2012) 014910 [arXiv:1107.4630] [INSPIRE].

[27] J. Nystrand for the ALICE collaboration, *Photonuclear production of vector mesons in ultra-peripheral Pb-Pb collisions at the LHC*, *Nucl. Phys.* **A 931** (2014) 298 [arXiv:1408.0811] [INSPIRE].

[28] C. Ewerz, M. Maniatis and O. Nachtmann, *A model for soft high-energy scattering: tensor pomeron and vector odderon*, *Annals Phys.* **342** (2014) 31 [arXiv:1309.3478] [INSPIRE].

[29] L. Lukaszuk and B. Nicolescu, *A possible interpretation of pp rising total cross-sections*, *Lett. Nuovo Cim.* **8** (1973) 405 [INSPIRE].

[30] D. Joynson, E. Leader, B. Nicolescu and C. Lopez, *Non-Regge and hyper-Regge effects in pion-nucleon charge exchange scattering at high-energies*, *Nuovo Cim.* **A 30** (1975) 345 [INSPIRE].

[31] C. Ewerz, *The odderon in quantum chromodynamics*, hep-ph/0306137 [INSPIRE].

[32] A. Schäfer, L. Mankiewicz and O. Nachtmann, *Diffractive η_c, η', J/ψ and ψ' production in electron-proton collisions at HERA energies*, in the proceedings of the workshop *Physics at HERA*, Hamburg, Germany (1991) volume 1, p. 243.

[33] V.V. Barakhovsky, I.R. Zhitnitsky and A.N. Shelkovenko, *Odderon: a sharp signal at HERA*, *Phys. Lett.* **B 267** (1991) 532 [INSPIRE].

[34] W. Kilian and O. Nachtmann, *Single pseudoscalar meson production in diffractive ep scattering*, *Eur. Phys. J.* **C 5** (1998) 317 [hep-ph/9712371] [INSPIRE].

[35] E.R. Berger et al., *Odderon and photon exchange in electroproduction of pseudoscalar mesons*, *Eur. Phys. J.* **C 9** (1999) 491 [hep-ph/9901376] [INSPIRE].

[36] E.R. Berger, A. Donnachie, H.G. Dosch and O. Nachtmann, *Observing the odderon: tensor meson photoproduction*, *Eur. Phys. J.* **C 14** (2000) 673 [hep-ph/0001270] [INSPIRE].

[37] S.J. Brodsky, J. Rathsman and C. Merino, *Odderon-pomeron interference*, *Phys. Lett.* **B 461** (1999) 114 [hep-ph/9904280] [inSPIRE].

[38] I.P. Ivanov, N.N. Nikolaev and I.F. Ginzburg, *Possible odderon discovery at HERA via charge asymmetry in the diffractive $\pi^+\pi^-$ production*, in the proceedings of the 9th *international workshop on Deep Inelastic Scattering (DIS 2001)*, April 27–May 1, Bologna, Italy (2001), hep-ph/0110181 [inSPIRE].

[39] P. Hägler, B. Pire, L. Szymanowski and O.V. Teryaev, *Hunting the QCD odderon in hard diffractive electroproduction of two pions*, *Phys. Lett.* **B 535** (2002) 117 [*Erratum ibid.* **B 540** (2002) 324] [hep-ph/0202231] [inSPIRE].

[40] P. Hägler, B. Pire, L. Szymanowski and O.V. Teryaev, *The charge asymmetry from pomeron-odderon interference in hard diffractive $\pi^+\pi^-$ electroproduction*, *Nucl. Phys.* **A 711** (2002) 232 [hep-ph/0206270] [inSPIRE].

[41] P. Hägler, B. Pire, L. Szymanowski and O.V. Teryaev, *Pomeron-odderon interference effects in electroproduction of two pions*, *Eur. Phys. J.* **C 26** (2002) 261 [hep-ph/0207224] [inSPIRE].

[42] I.F. Ginzburg, I.P. Ivanov and N.N. Nikolaev, *Possible odderon discovery via observation of charge asymmetry in the diffractive $\pi^+\pi^-$ production at HERA*, *Eur. Phys. J. direct* **C 5** (2003) 02 [hep-ph/0207345] [inSPIRE].

[43] I.F. Ginzburg, *Charge asymmetry in e^+e^-, ep, $e\gamma$, $\gamma\gamma$ collisions*, hep-ph/0211099 [inSPIRE].

[44] I.F. Ginzburg and I.P. Ivanov, *How to measure pomeron phase and discover odderon at HERA and RHIC*, *Acta Phys. Polon.* **B 37** (2006) 841 [hep-ph/0512174] [inSPIRE].

[45] H. Primakoff, *Photo-production of neutral mesons in nuclear electric fields and the mean life of the neutral meson*, *Phys. Rev.* **81** (1951) 899 [inSPIRE].

[46] H1 collaboration, C. Adloff et al., *Search for odderon induced contributions to exclusive π^0 photoproduction at HERA*, *Phys. Lett.* **B 544** (2002) 35 [hep-ex/0206073] [inSPIRE].

[47] T. Berndt for the H1 collaboration, *Investigation of pomeron and odderon induced photoproduction of mesons decaying to pure multiphoton final states at HERA*, *Acta Phys. Polon.* **B 33** (2002) 3499 [inSPIRE].

[48] A. Donnachie, H.G. Dosch and O. Nachtmann, *The missing odderon*, *Eur. Phys. J.* **C 45** (2006) 771 [hep-ph/0508196] [inSPIRE].

[49] C. Ewerz and O. Nachtmann, *Chiral symmetry and diffractive neutral pion photo- and electroproduction*, *Eur. Phys. J.* **C 49** (2007) 685 [hep-ph/0608082] [inSPIRE].

[50] P.D.B. Collins, *An introduction to Regge theory and high-energy physics*, Cambridge University Press, Cambridge U.K. (1977).

[51] P.D.B. Collins and A.D. Martin, *Hadron interactions*, Adam Hilger, Bristol U.K. (1984).

[52] V.N. Gribov, Y.L. Dokshitzer and J. Nyiri, *Strong interactions of hadrons at high energies: Gribov lectures on theoretical physics*, Cambridge University Press, Cambridge U.K. (2009).

[53] P. Söding, *On the apparent shift of the ρ meson mass in photoproduction*, *Phys. Lett.* **19** (1966) 702 [inSPIRE].

[54] S.D. Drell, *Production of particle beams at very high energies*, *Phys. Rev. Lett.* **5** (1960) 278 [inSPIRE].

[55] S.D. Drell, *Peripheral contributions to high-energy interaction processes*, *Rev. Mod. Phys.* **33** (1961) 458 [INSPIRE].

[56] P. Lebiedowicz, O. Nachtmann and A. Szczurek, *The ρ^0 and Drell-Söding contributions to central exclusive production of $\pi^+\pi^-$ pairs in proton-proton collisions at high energies*, arXiv:1412.3677 [INSPIRE].

[57] R. Mertig, M. Böhm and A. Denner, *FEYN CALC: computer algebraic calculation of Feynman amplitudes*, *Comput. Phys. Commun.* **64** (1991) 345 [INSPIRE].

[58] A.C. Limache and P.S. Rojas Fredini, *LTensor: a high performance C++ tensor library based on index notation*, http://code.google.com/p/ltensor/.

[59] R. Brun and F. Rademakers, *ROOT: an object oriented data analysis framework*, *Nucl. Instrum. Meth.* **A 389** (1997) 81 [INSPIRE], see also http://root.cern.ch.

[60] F.J. Gilman, J. Pumplin, A. Schwimmer and L. Stodolsky, *Helicity conservation in diffraction scattering*, *Phys. Lett.* **B 31** (1970) 387 [INSPIRE].

[61] K. Schilling, P. Seyboth and G.E. Wolf, *On the analysis of vector meson production by polarized photons*, *Nucl. Phys.* **B 15** (1970) 397 [*Erratum ibid.* **B 18** (1970) 332] [INSPIRE].

[62] K. Schilling and G. Wolf, *How to analyze vector meson production in inelastic lepton scattering*, *Nucl. Phys.* **B 61** (1973) 381 [INSPIRE].

[63] P. Lebiedowicz, O. Nachtmann and A. Szczurek, *Exclusive central diffractive production of scalar and pseudoscalar mesons: tensorial vs. vectorial pomeron*, *Annals Phys.* **344** (2014) 301 [arXiv:1309.3913] [INSPIRE].

[64] K. Gottfried and J.D. Jackson, *On the connection between production mechanism and decay of resonances at high-energies*, *Nuovo Cim.* **33** (1964) 309 [INSPIRE].

[65] J.D. Jackson, *Remarks on the phenomenological analysis of resonances*, *Nuovo Cim.* **34** (1964) 1644 [INSPIRE].

[66] J.C. Collins and D.E. Soper, *Angular distribution of dileptons in high-energy hadron collisions*, *Phys. Rev.* **D 16** (1977) 2219 [INSPIRE].

[67] E. Byckling and K. Kajantie, *Particle kinematics*, J. Wiley, London U.K. (1973).

[68] D. Melikhov, O. Nachtmann, V. Nikonov and T. Paulus, *Masses and couplings of vector mesons from the pion electromagnetic, weak and $\pi\gamma$ transition form factors*, *Eur. Phys. J.* **C 34** (2004) 345 [hep-ph/0311213] [INSPIRE].

[69] PARTICLE DATA GROUP collaboration, J. Beringer et al., *Review of particle physics*, *Phys. Rev.* **D 86** (2012) 010001 [INSPIRE].

[70] J.H. Kühn and A. Santamaria, *Tau decays to pions*, *Z. Phys.* **C 48** (1990) 445 [INSPIRE].

[71] ZEUS collaboration, H. Abramowicz et al., *Exclusive electroproduction of two pions at HERA*, *Eur. Phys. J.* **C 72** (2012) 1869 [arXiv:1111.4905] [INSPIRE].